iScience

CellPress

Article

Clostridium butyricum Modulates the Microbiome to Protect Intestinal Barrier Function in Mice with Antibiotic-Induced Dysbiosis

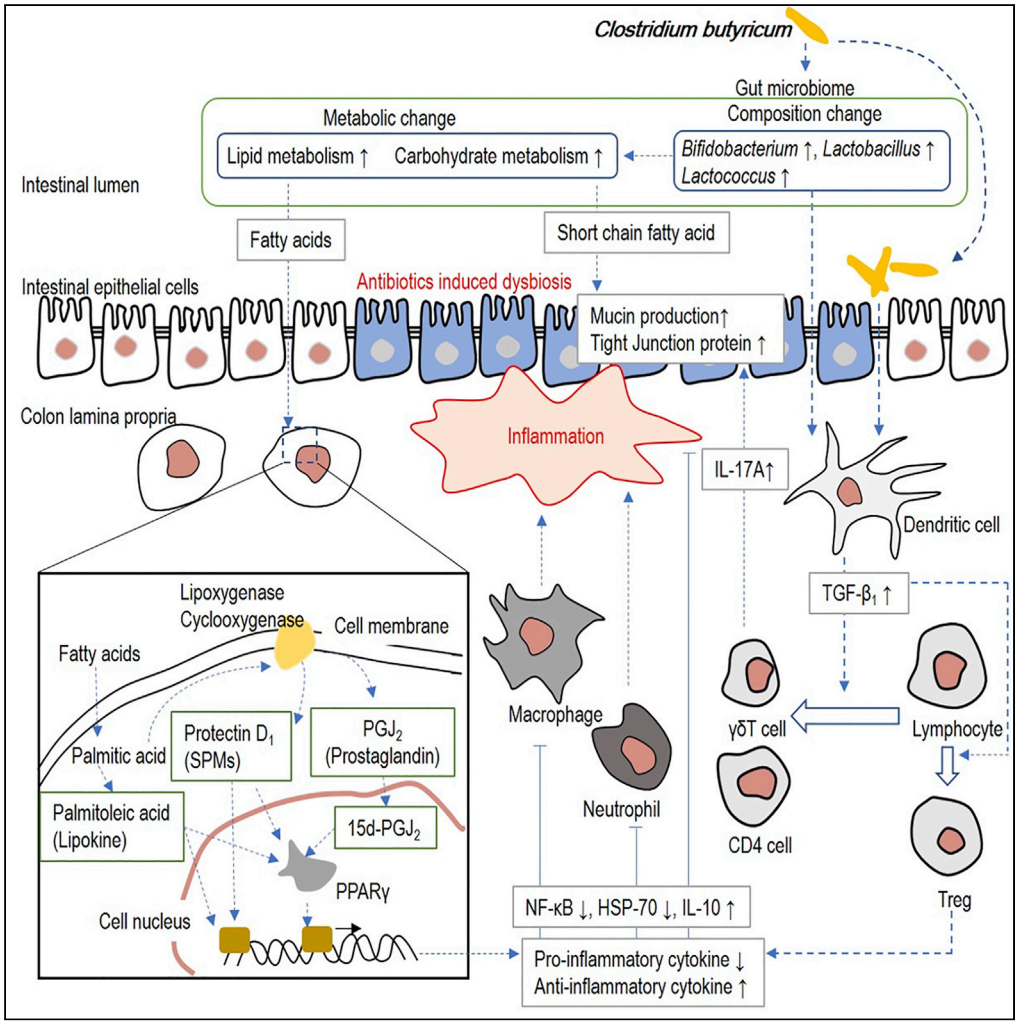

Mao Hagihara, Yasutoshi Kuroki, Tadashi Ariyoshi, ..., Yuka Yamagishi, Motomichi Takahashi, Hiroshige Mikamo

mikamo@aichi-med-u.ac.jp

HIGHLIGHTS

CBM 588 increases the abundance of *Bifidobacterium*, *Lactobacillus*, and *Lactococcus*

Microbiota-driven TGF-β_1 controls the differentiation of lymphocytes to γδT cells

CBM 588 promotes the expansion of IL-17A-producing γδT cells and CD4 cells

CBM 588 upregulates anti-inflammatory lipid metabolites

Hagihara et al., iScience *23*, 100772
January 24, 2020
https://doi.org/10.1016/j.isci.2019.100772

iScience

CellPress

Article

Clostridium butyricum Modulates the Microbiome to Protect Intestinal Barrier Function in Mice with Antibiotic-Induced Dysbiosis

Mao Hagihara,[1] Yasutoshi Kuroki,[2,3] Tadashi Ariyoshi,[2,3] Seiya Higashi,[3] Kazuo Fukuda,[3] Rieko Yamashita,[1] Asami Matsumoto,[3] Takeshi Mori,[2] Kaoru Mimura,[4] Naoko Yamaguchi,[4] Shoshiro Okada,[4] Tsunemasa Nonogaki,[5] Tadashi Ogawa,[6] Kenta Iwasaki,[7] Susumu Tomono,[8] Nobuhiro Asai,[2] Yusuke Koizumi,[2] Kentaro Oka,[2,3] Yuka Yamagishi,[2] Motomichi Takahashi,[2,3] and Hiroshige Mikamo[2,9,*]

SUMMARY

***Clostridium butyricum* MIYAIRI 588 (CBM 588) is a probiotic bacterium that has previously been used to prevent antibiotic-associated diarrhea. However, the underlying mechanism by which CBM 588 protects the gut epithelial barrier remains unclear. Here, we show that CBM 588 increased the abundance of *Bifidobacterium*, *Lactobacillus*, and *Lactococcus* species in the gut microbiome and also enhanced the intestinal barrier function of mice with antibiotic-induced dysbiosis. Additionally, CBM 588 significantly promoted the expansion of IL-17A-producing γδT cells and IL-17A-producing CD4 cells in the colonic lamina propria (cLP), which was closely associated with changes in the intestinal microbial composition. Additionally, CBM 588 plays an important role in controlling antibiotic-induced gut inflammation through upregulation of anti-inflammatory lipid metabolites such as palmitoleic acid, 15d-prostaglandin J_2, and protectin D_1. This study reveals a previously unrecognized mechanism of CBM 588 and provides new insights into gut epithelial barrier protection with probiotics under conditions of antibiotic-induced dysbiosis.**

INTRODUCTION

The intestinal microbiota contributes to many host physiological processes, including nutrient acquisition, development of the gut-specific immune system, and protection from infectious pathogens. To maintain a mutually beneficial relationship between the host and commensal microorganisms, the host immune system shapes the compositional balance of symbiotic commensal bacteria (Hooper et al., 2012). Recent studies have revealed that an imbalance in bacterial composition (dysbiosis) triggers a host pro-inflammatory immune response and induces various inflammatory and metabolic diseases (Elinav et al., 2011; Garrett et al., 2007; Vijay-Kumar et al., 2010).

Widespread antibiotic exposure is associated with a variety of gastrointestinal effects, hypersensitivity, and drug-specific adverse effects, most notable of which is antibiotic-associated diarrhea (AAD) in 5%–35% of treated patients (Wiström et al., 2001; McFarland, 2014). Non-selective antibiotic-induced dysbiosis accounts for up to 20% of all AAD cases (Bartlett, 2002). Probiotics have been proposed to constitute an effective preventive treatment for antibiotic-induced dysbiosis and associated adverse effects in mice (Ekmekciu et al., 2017; Hempel et al., 2012). Multiple *in vitro* studies have confirmed that probiotics can prevent an increase in colon epithelial cell permeability and can play a role in repairing damage to the intestinal epithelial barrier (Johnson-Henry et al., 2008; Resta-Lenert and Barrett, 2006).

The gram-positive obligate anaerobic bacillus, *Clostridium butyricum* (CB), exists in the soil, and in animal and human intestines. Specifically, *Clostridium butyricum* MIYAIRI 588 (CBM 588) is a probiotic bacterium that has been used in the treatment of various human gastrointestinal diseases in Japanese clinical settings (Seki et al., 2003). Our previous *in vivo* study showed that treatment with CBM 588 reduced gut epithelial damage caused by antibiotic administration, in addition to reducing superficial epithelial necrosis and the presence of inflammatory cells (Hagihara et al., 2018). Other studies have suggested that CBM 588 can directly supplement butyrate during the repair of damaged intestinal mucosa, as a kind of butyrate-producing probiotic (Dnucan et al., 2002). An *in vivo* study demonstrated that CBM 588 also induces intestinal IL-10-producing macrophages to suppress acute experimental colitis induced by dextran sulfate sodium

[1]Department of Molecular Epidemiology and Biomedical Sciences, Aichi Medical University, Nagakute 480-1195, Japan

[2]Department of Clinical Infectious Diseases, Aichi Medical University, Nagakute 480-1195, Japan

[3]Miyarisan Pharmaceutical Co., Ltd., Saitama 114-0016, Japan

[4]Department of Pharmacology, Aichi Medical University, Nagakute 480-1195, Japan

[5]Department of Pharmacy, College of Pharmacy Kinjo Gakuin University, Nagoya 463-8521, Japan

[6]Department of Legal Medicine, Aichi Medical University, Nagakute 480-1195, Japan

[7]Departments of Kidney Disease and Transplant Immunology, Aichi Medical University, Nagakute 480-1195, Japan

[8]Department of Microbiology and Immunology, Aichi Medical University, Nagakute 480-1195, Japan

[9]Lead Contact

*Correspondence: mikamo@aichi-med-u.ac.jp

https://doi.org/10.1016/j.isci.2019.100772

(DSS) (Hayashi et al., 2013). However, the underlying mechanism by which CBM 588 protects the gut epithelial barrier remains unclear both during and after antibiotic treatment.

To elucidate this mechanism, we investigated the immunological and metabolic interaction between the host and gut microbiome under antibiotic-induced dysbiosis. This work reveals two novel protective mechanisms of epithelial cells in the colon under CBM 588 treatment. First, CBM 588 induces IL-17A-producing γδT cells and IL-17A-producing CD4 cells in the colonic lamina propria (cLP), thus enhancing gut epithelial barrier function under antibiotic-induced dysbiosis. Second, CBM 588 plays an important role in controlling antibiotic-induced gut inflammation through upregulation of anti-inflammatory lipid metabolites such as palmitoleic acid, 15d-prostaglandin J_2, and protectin D_1. This study provides new insights into gut epithelial barrier protection with probiotics under conditions of antibiotic-induced dysbiosis.

RESULTS

Antibiotics Compromise Gut Epithelial Integrity

Mounting evidence suggests that commensal *Clostridium* strains have major effects on the development of the gut immune system, thereby regulating gut homeostasis (Atarashi et al., 2011; Ivanov et al., 2009). Although CBM 588 has a major impact on the treatment of gastrointestinal diseases, the precise mechanism by which it prevents epithelial damage remains to be elucidated. To determine whether colonization by CBM 588 has an immunomodulatory and metabolic role in regulating gut homeostasis, we administered clindamycin and/or CBM 588 to ICR mice for 4 days (Figure 1A). We confirmed that colonization of CB was retained in the colon even after clindamycin administration (Figure 1B). The spore colony counts for the CBM 588 administration group and combination (clindamycin + CBM 588) group were similar to the total CB colony count in each group throughout the study period. The CBM 588 administration group showed the highest CB colony counts at day 2, and the counts rapidly decreased after CBM 588 administration was discontinued. During the treatment period, CB counts also increased in the combination group and decreased after CBM 588 administration was discontinued. However, bacterial regrowth was observed in the combination group, and the highest CB colony counts were on day 8. During the study period, CBM 588 showed a slight effect on body weight and no effects on stool consistency. The body weight of ICR mice was increased by CBM 588 administration and was not attenuated in mice given clindamycin (Figure 1C). Macroscopic findings revealed a slightly shortened colon length in mice administered CBM 588 (Figure 1D). We expected the clindamycin administration group to show shorter colon compared with the other group. However, our study showed the opposite result with previous *in vivo* study with colitis model induced by DSS, whereas the reason was unclear (Hayashi et al., 2013). In histological examination, only the clindamycin administration group samples showed abnormalities at day 8, such as (1) superficial epithelial necrosis and (2) presence of inflammatory cells, including mainly neutrophil infiltration (Figure 1E). In contrast, CBM 588 administration group samples showed histologically normal colon mucosa, even though clindamycin was administered concurrently. Compared with the control and CBM 588 groups, the clindamycin administration group showed a significantly higher histological inflammation score (Figure 1F). Although there was no significant difference, the combination group showed a numerically lower score than that of the clindamycin administration group. Additionally, we also noticed that the clindamycin administration group had significantly more epithelial damage in the colon (Figure 1G). Protective effects of CBM 588 on colon mucosa have also been observed in the acute DSS colitis model (Hayashi et al., 2013). Similar to our previous study (Hagihara et al., 2018), we found that CBM 588 administration prevented the development of clindamycin-induced colitis. However, the mechanism by which CBM 588 protects the colon from antibiotic damage remains unclear. To address this, we assessed gut microbiome, cytokine profiles in isolated colon tissue, and metabolic profile alternations in gut microbiome and host gut colon tissue.

CBM 588 Modulates the Gut Microbiome Composition under Clindamycin-Induced Dysbiosis

To reveal the impact of CBM 588 on the gut microbiome under antibiotic treatment conditions, we conducted gut microbiome analysis. Changes to the murine gut microbiome at the phylum level, after either 4 or 8 days, is shown in Figure 2A. Bar graphs depict the mean percent abundances of bacterial families (≥1% relative abundance). Intestinal flora mainly consisted of members of the Firmicutes (Clostridiales, Lactobacillus) and Bacteroidetes phyla (Bacteroidales, Bacteroides) in the control group and CBM 588-administered group, respectively. Clindamycin administration resulted in dramatic increases in Proteobacteria phylum. However, the presence of members of the Bacteroidetes phylum dramatically decreased, and

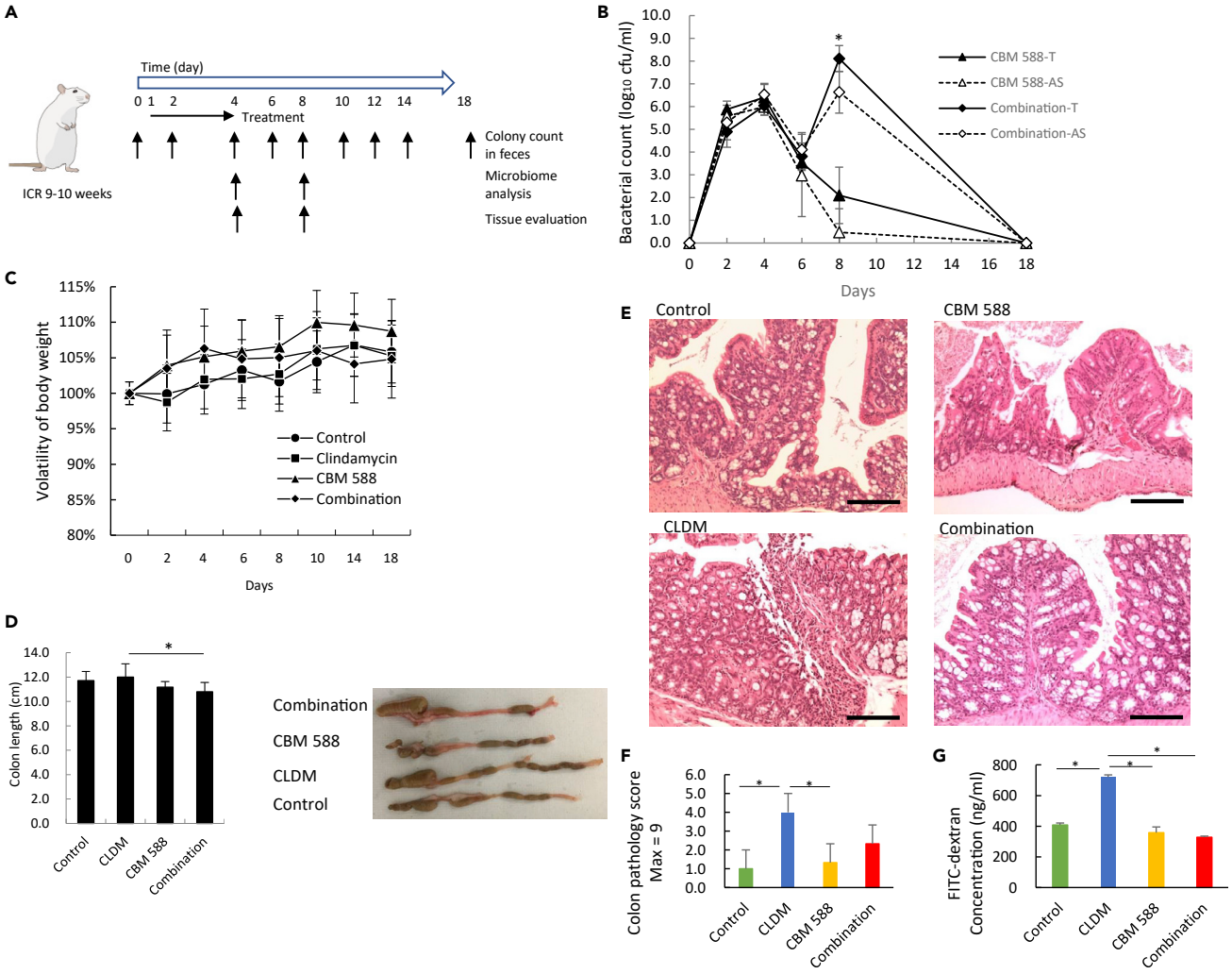

Figure 1. Mice Suffer Worse Epithelial Injury after Clindamycin Administration

(A) Experimental design of clindamycin and/or CBM 588 administration in 9- to 10-week-old ICR mice. Mice received clindamycin and/or CBM 588 via sonde for 4 days; 1: control group (Control), 2: clindamycin administration group (CLDM), 3: CBM 588 administration group (CBM 588), and 4: combination (CBM 588 + clindamycin) group (Combination). Collection time points of stool for *C. butyricum* colony count and microbiome analysis and colon tissue for cytokine and macroscopic analysis are indicated.

(B) Enumerating *C. butyricum* in feces in ▲: total colony count in CBM 588 administration group (CBM 588-T), △: spore colony count in CBM 588 monotherapy group (CBM 588-AS), ●: total colony count in combination group (Combination-T), ○: spore colony count in combination group (Combination-AS). The testing detectable level is above 2.3 (log amount) in per gram feces, with representative data n = 5–10 per group, mean ± SEM. Statistical analysis of quantitative multiple group comparisons was performed using a one-way analysis of variance followed by Tukey's test, *$p < 0.05$.

(C) Weight changes of control group (●), CBM 588 administration group (▲), clindamycin administration group (■), and combination group (◆) for mice over time duration of the study (18 days), with representative data n = 5 per group, mean ± SEM.

(D) Colon length (cm) at day 8, with representative data n = 5 per group, mean ± SEM. Pictures show representative isolated colons from each group. Statistical analysis of the quantitative multiple group comparisons was performed using a one-way analysis of variance followed by Tukey's test, *$p < 0.05$.

(E) Hematoxylin and eosin (H&E) staining of colons at day 8 revealed superficial epithelial necrosis and the presence of inflammatory cells only in the clindamycin administration group (magnification, 10× and the scale bar represents 150 μm).

(F) Histopathology scoring of H&E-stained colon sections in each group mice. All values are mean ± SEM (n = 5). Statistical analysis of the quantitative multiple group comparisons was performed using a one-way analysis of variance followed by Tukey's test, *$p < 0.05$.

(G) Intestinal permeability was determined. All values are mean ± SEM (n = 5). Statistical analysis of the quantitative multiple group comparisons was performed using a one-way analysis of variance followed by Tukey's test, *$p < 0.05$.

Firmicutes phylum members also decreased, although a dramatic increase was observed at day 8. Gut microbiome modification for the combination group was similar to that of the clindamycin administration group, at the phylum level.

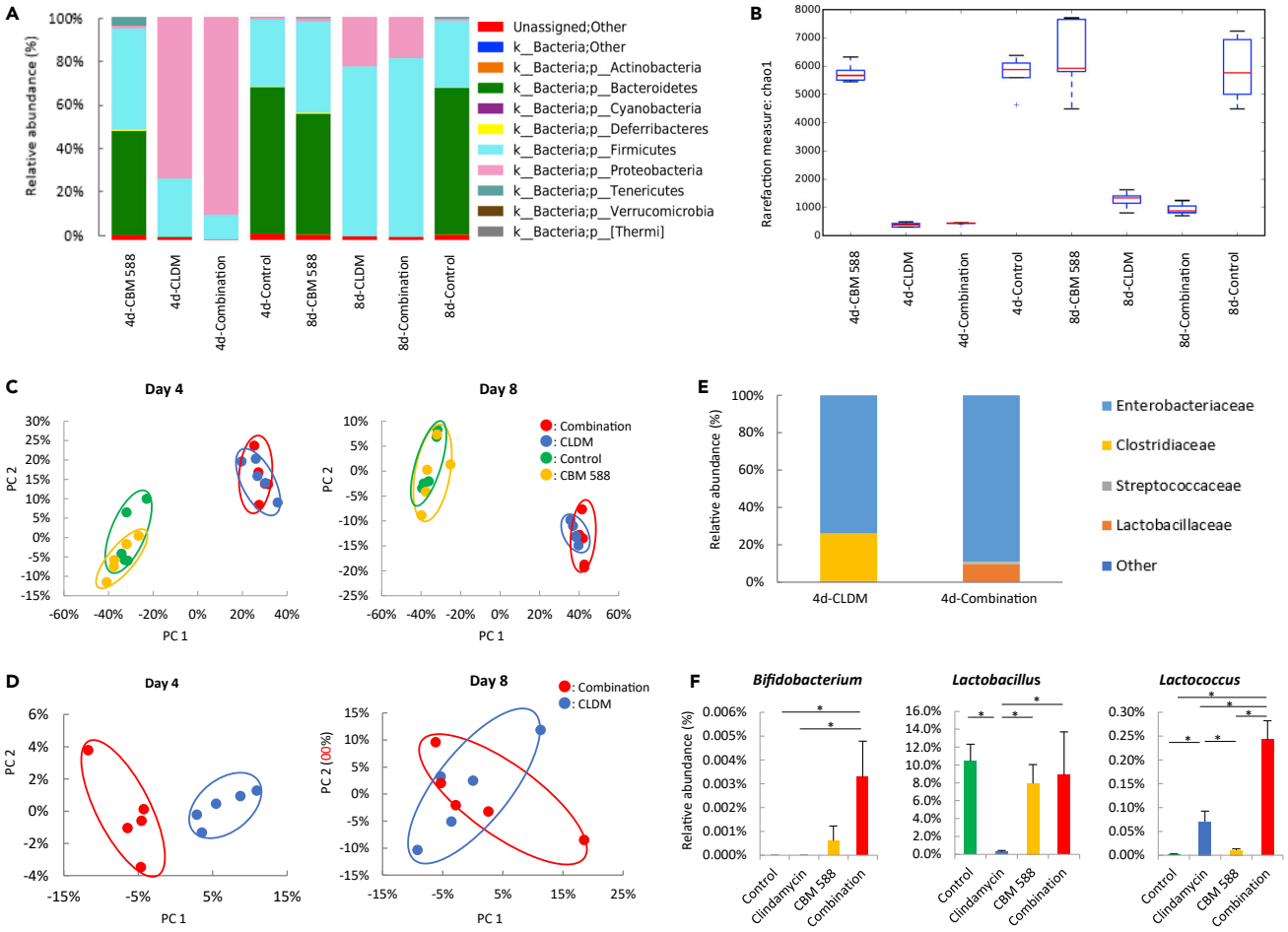

Figure 2. CBM 588 Modulates Gut Bacterial Composition in Mice

(A) Bacterial compositions in different experimental groups at the phylum level. 4d: sampling at day 4, 8d: sampling at day 8.

(B) Comparison of the Shannon index of different groups. The box and whiskers represent the smallest and largest values, with the median in the center of each box.

(C) Principal Coordinate Analysis (PCoA) based on weighted Unifrac distances among four groups.

(D) PCoA based on weighted Unifrac distances between the clindamycin administration group and the combination group.

(E) The bacterial composition at day 4 in the clindamycin administration group and combination group at the family level.

(F) Effect of clindamycin and CBM 588 administrations on relative species abundance (≥0.001%) in the fecal samples. After quality filtering steps, three species (*Bifidobacterium*, *Lactobacillus*, and *Lactococcus*) were considered to have significantly higher relative abundance (%) in the combination group, compared with the clindamycin administration group at day 4. Data represent the mean values of relative abundances ±SEM (n = 5–10). Statistical analysis of the quantitative multiple group comparisons was performed using a one-way analysis of variance followed by Tukey's test, *p < 0.05.

To determine bacterial richness and diversity in the gut microbiome, we calculated α-diversity and β-diversity based on fecal samples for all groups. Clindamycin exposure significantly decreased α-diversity ($p < 0.05$) (Figure 2B). A similar trend was observed in bacterial α-diversity over time in both groups, as there were no significant differences between the clindamycin administration group and combination group. Also, both groups did not recover α-diversity during the study period. The control group and CBM 588 administration group exhibited stable scores in α-diversity at day 4 and day 8. At two time points, no significant difference in α-diversity was also observed between the control group and CBM 588 administration group. PCoA based on the weighted Unifrac distance metric is shown in Figure 2C. There was no significant change in bacterial community composition for the CBM 588 administration group and control group at day 4 and day 8. However, bacterial communities in the clindamycin administration groups (including the combination group) clustered separately ($p < 0.05$) from the control group at days 4 and 8 (Figure 2C), whereas bacterial communities in fecal samples of the clindamycin administration group and combination group did not cluster separately from each other at day 4 and day 8. However, bacterial communities of the

combination group clustered separately from the clindamycin group at day 4 ($p < 0.05$), when compared with only two groups (Figure 2D). These data suggest that the impact of clindamycin on the gut microbiome was much greater than that of CBM 588. However, CBM 588 does have some effect on the gut microbiome, since the microbial composition of the clindamycin administration group and combination group were different during the CBM 588 administration period, whereas differences were less when compared with the control group.

We then investigated murine gut microbiome changes at the genus and species level at day 4 (Figure S1). The relative abundance of various families with percentages of sequences $\geq$0.001% of the bacterial community was analyzed (Figure 2E). The intestinal flora mainly consisted of *Enterobacteriales* for the clindamycin administration group and combination group, and CBM 588 administration resulted in dramatic increases in the *Lactobacillales* and *Bifidobacteriales* genera. However, the *Clostridiales* genera were reduced in the combination group. The relative abundance (%) of three species (*Bifidobacterium*, *Lactobacillus*, and *Lactococcus*) in the combination group were significantly increased compared with that in the clindamycin administration group at day 4 (Figure 2F). *Bifidobacterium* abundance was increased in the combination group, but relative abundances of *Bifidobacterium* in the control and clindamycin administration groups were nearly zero during the study period. *Lactococcus* in the combination group showed a higher relative abundance at day 4 than that seen in the other groups. *Lactobacillus* for only the clindamycin administration group was reduced at day 4, and microbiome analysis revealed that clindamycin induced gut dysbiosis in mice. Microbiomes were similar at the phylum level between the clindamycin administration group and combination group. However, CBM 588 impacted the gut microbiome, and some species, such as *Bifidobacterium*, *Lactobacillus*, and *Lactococcus*, exhibited an inverse correlation between the combination group and clindamycin administration group. These results suggest that clindamycin administration reduces diversity in the gut microbiome, even with concurrent administration of CBM 588. However, the composition of the microbiome was significantly different between the clindamycin administration group and the combination group. Therefore, these results support the hypothesis that host physiological processes to maintain gut homeostasis are affected differently in the clindamycin group and combination group under CBM 588 treatment.

CBM 588 Modulates Cytokine Expression to Regulate Gut Inflammation under Antibiotic-Induced Dysbiosis

Next, we sought to elucidate the mechanisms of gut epithelial protection exerted by an altered gut microbiome after CBM 588 administration. To address this, we isolated colon tissues from mice and assessed cytokine profiles with qPCR (the sequences of primers are summarized in Table S1) and ELISA. CBM 588 is known to exhibit a colitis-preventing effect in different experimental colitis models (Hayashi et al., 2013), and a previous study revealed that CBM 588 promotes Treg cell generation through induction of transforming growth factor β_1 (TGF-β_1) by dendritic cells (DCs) in a DSS-induced acute colitis model (Kashiwagi et al., 2015). Consistent with this previous report (Kashiwagi et al., 2015), CBM 588 administration enhanced the expression of TGF-β_1 RNA (Figure 3A) and TGF-β_1 protein (Figure 3B), compared with the clindamycin administration group and control group in this study. Although CBM 588-mediated TGF-β_1 induction was mainly Toll-like receptor-2 (TLR-2) dependent, and the ERK-AP-1 kinase pathway played an important role (Kashiwagi et al., 2015), our study revealed that TLR-2 RNA expression levels increased with CBM 588 administration (Figure 3C).

Additionally, we found that various inflammatory cytokines were upregulated in the clindamycin administration group (Figures 3D and S2). However, consistent with previous report findings for the concurrent administration of CBM 588 (Hayashi et al., 2013), we found that CBM 588 reduced RNA expression levels of inflammatory cytokines, including interleukin-1β, IL-6, interferon-γ (INF-γ), cyclooxygenase-2 (COX-2), and tumor necrosis factor alpha (TNF-α), while increasing IL-10 RNA expression levels in colonic tissue on day 8 after antibiotic treatment (Figure 3D). Likewise, TNF-α protein levels were also reduced with CBM 588 administration (Figure 3E). Another previous study revealed that the TGF-β_1 pathway regulates inflammatory cytokines and promotes IL-10 cytokine production (Hayashi et al., 2013; Huang et al., 2013). These data suggest that the anti-inflammatory effect of CBM 588 on clindamycin-induced colitis is associated with a TGF-β_1-dependent reduction of inflammatory cytokine expression and increase in anti-inflammatory cytokines. Also, for the CBM 588 administration groups, including the combination group, regulation of NF-κB and HSP-70 RNA expression levels was observed (Figure 3F). Although

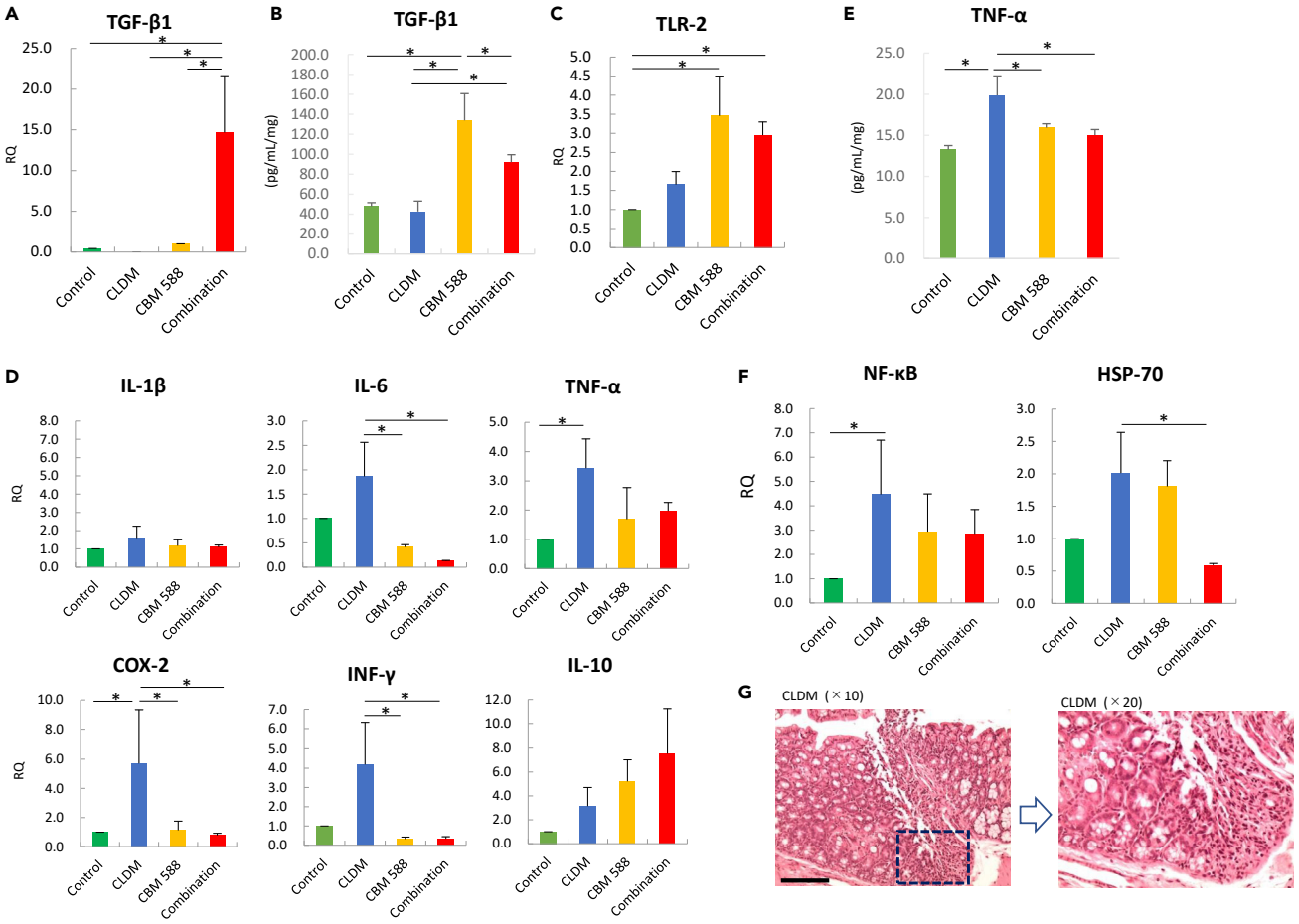

Figure 3. CBM 588 Modulates Inflammation and Anti-inflammation Cytokines to Suppress Antibiotic-Induced Colitis

(A) The relative RNA expression levels of genes encoding TGF-β_1 in colon tissue of mice detected at day 8 by qPCR.

(B) TGF-β_1 protein concentrations in colon tissues of mice detected at day 8 by ELISA.

(C) The relative RNA expression levels of genes encoding TLR-2 in colon tissue of mice detected at day 8, as detected by qPCR.

(D) The relative RNA expression levels of genes encoding IL-1β, IL-6, TNF-α, COX-2, INF-γ, and IL-10 in colon tissue of mice at day 8, as detected by qPCR.

(E) TNF-α protein concentrations in colon tissues of mice detected at day 8, as measured by ELISA.

(F) The relative RNA expression levels of genes encoding NF-κB and HSP-70 in colon tissue of mice detected at day 8, measured by qPCR.

(G) Hematoxylin and eosin (H&E) staining of colons in the clindamycin group shows the presence of inflammatory cells at day 8, including many neutrophil infiltration after clindamycin administration (left: magnification, 10× and the scale bar represents 150 μm) (right: magnification, 20×).

All values are mean ± SEM (n = 5–10). Statistical analysis of the quantitative multiple group comparisons was performed using a one-way analysis of variance followed by Tukey's test, *p < 0.05.

RNA expression is not the standard method used to assess NF-κB activation, these results might support a suppressive effect of CBM 588 on the migration and infiltration of leukocytes in the colon tissue (Figure 3G). In addition, antibiotic-induced dysbiosis occurs rapidly within several days, leading to altered bacterial metabolism and an impaired host proteome in mice and humans (Ferrer et al., 2014; Lichtman et al., 2016). Taken together, we found that clindamycin administration caused gut inflammation and CBM 588 modulated gut cytokine expression under antibiotic-induced dysbiosis through the TGF-β_1 pathway, which is similar to previous studies using other murine DSS-induced colitis models (Kashiwagi et al., 2015; Hayashi et al., 2013). However, this signaling pathway did not enhance IgA antibody production from Treg cells in this study (Figure S3), which was like a previous study using a DSS-induced colitis model (Kashiwagi et al., 2015). The reduction of some inflammatory cytokines in the CBM 588 administration groups indicates that CBM 588 may have an effect on tight junction proteins of epithelial columnar cells and may change metabolic profiles in colonic tissue to reduce inflammation.

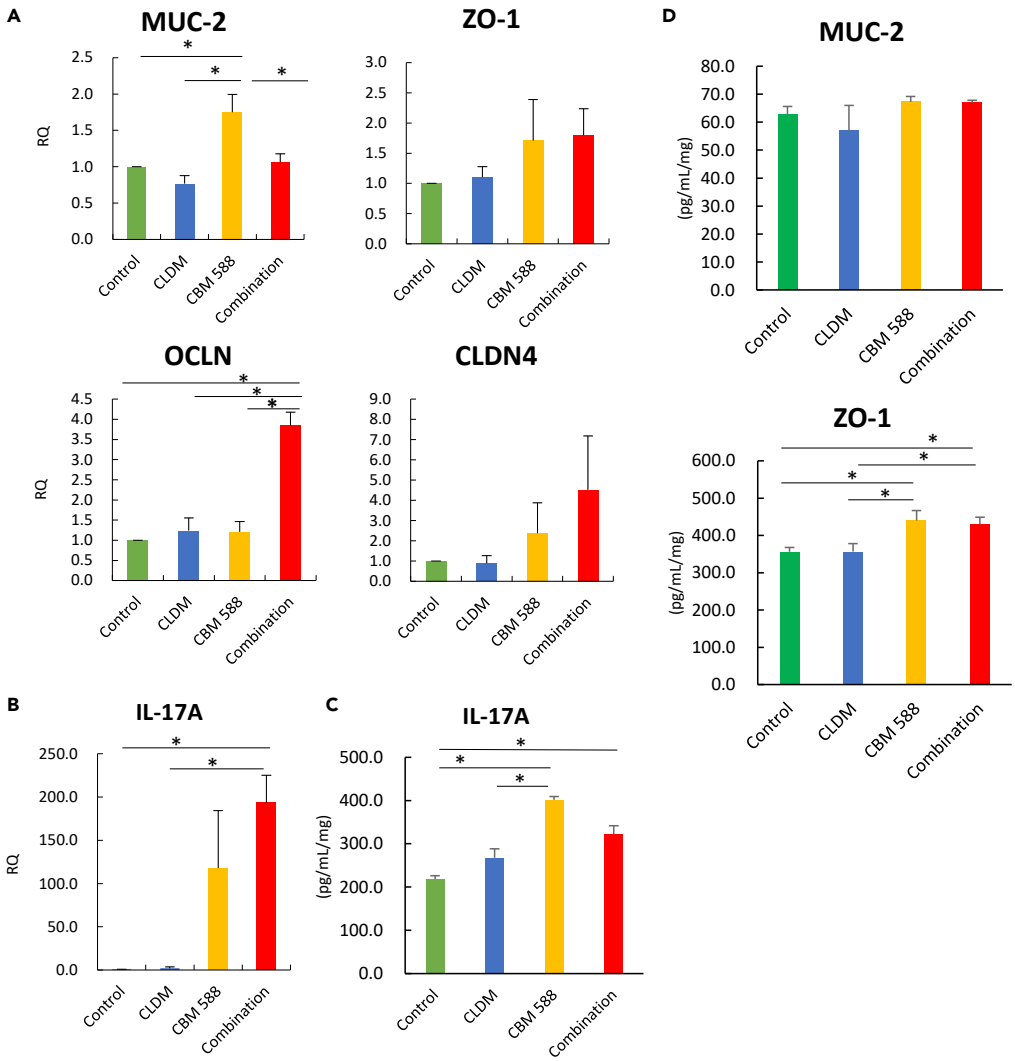

Figure 4. CBM 588 Enhances Intestinal Barrier Function of Colitis Mice

(A) The relative RNA expression of genes encoding mucin-2 (MUC-2), claudin (CLDN4), zonula occludens (ZO-1), and occludin (OCLN) in colon tissues of mice, detected by qPCR.

(B) The relative RNA expression levels of genes encoding IL-17A in colon tissues of mice, detected by qPCR.

(C) The IL-17A concentration in each animal group was detected by ELISA.

(D) The MUC-2 and ZO-1 concentrations in each animal group were detected by ELISA.

All values are mean ± SEM (n = 5–10). Statistical analysis of the quantitative multiple group comparisons was performed using a one-way analysis of variance followed by Tukey's test, *p < 0.05.

CBM 588 Promotes the Expansion of IL-17A-Producing γδT Cells and CD4 Cells in Colonic Lamina Propria to Maintain Gut Epithelial Barrier Integrity

The intestinal barrier is established by epithelial columnar cells and is built of monolayered columnar epithelial cells that are tightly connected by tight junction proteins (TJs) such as occludin (OCLD), zonula occludens-1 (ZO-1), and claudins-4 (CLDN4) (Whibley and Gaffen, 2015). TJs are the structural feature that help prevent the entry of laminal antigens and microorganisms (Deitch, 2002). The secretory protein mucin-2 (MUC-2) is also the primary component of the protective mucous layer in the colon (Willemsen et al., 2003). To further characterize the protective effects of CBM 588 on the epithelial layer during antibiotic administration in mice, we determined MUC-2, ZO-1, CLDN4, and OCLN RNA expression levels in mouse colon tissue by qPCR. Our results indicate that CBM 588 upregulated RNA expression levels for all these genes (Figure 4A). CBM 588 administration also enhanced MUC-2 and ZO-1 protein expressions (Figure 4D). Although TJs are normally considered part of the physical barrier, they are largely affected by

mucosal immune homeostasis within cLP as well as the composition of gut microbes and thus can be regarded as a translator between the microbiome and immune system (Martini et al., 2017; Ni et al., 2017; Alvarez et al., 2016). Several studies have revealed impaired TJ complexity and the downregulation of TJs in ulcerative colitis (UC), which could be a mechanism contributing to dysfunction of the intestinal barrier. In this study, CBM 588 increased mucin production and TJ expression levels, which have been found to lead to greater epithelial barrier integrity (Pastorelli et al., 2013; Perse and Cerar, 2012).

Moreover, previous studies have shown that, after acute intestinal injury, the intestinal-protective cytokine IL-17A could regulate TJs to limit excessive permeability and maintain barrier integrity (Lee et al., 2015). We therefore tested IL-17A RNA expression levels and IL-17A protein levels in the colon tissue and found that CBM 588 induced an increase in IL-17A levels in colon tissue at day 8 (Figures 4B and 4C). Mucosal T cells in cLP are master cells that play an important role in maintaining intestinal barrier homeostasis. Among the immune cells dwelling in intestinal mucosa, γδT cells are rare T cell subsets that have been found to be involved in both pathogenic and protective networks in inflammatory bowel disease (IBD) (Paul et al., 2015). γδT cells in intestinal LP were found to be the major source of gut-protective IL-17A, and this γδT cell-derived IL-17A was found to promote the repair of damaged intestinal epithelium through adaptor molecule Act1-mediated regulation of TJ subcellular localization (Lee et al., 2015). Therefore, we hypothesized that IL-17A-producing γδT cells may be involved in the protective mechanism of CBM 588 on colon mucosa. IL-17A-producing γδT cells provide an immediate source of IL-17A at barrier sites, which supports a pro-inflammatory immune function. To investigate whether protective effects of CBM 588 were associated with the upregulation of IL-17A-producing γδT cells, we further isolated the lymphocytes in cLP and found an upregulation of γδT cells and IL-17A-producing γδT cells in the mouse combination group (Figures 5A and 5B), whereas no IL-17A-producing γδT cells were detected in the clindamycin administration group ($p < 0.05$). Additionally, as some other immune cells can produce IL-17A, such as Th17 cells and ILC3, we conducted additional evaluations of IL-17-producing CD8, CD4, and ILC3 cells in lamina propria (Figures 5C, 5D, S4A, and S4B) to clarify that CBM 588 affects other IL-17-producing cell populations. Consequently, CBM 588 were associated with the upregulation of CD4 cells and IL-17A-producing CD4 cells (Figure 5D). On the other hand, CD8 cell and ILC3 cell frequencies were not changed with CBM 588 (data not shown). Previous study results revealed that IL-17A produced by γδT cells and CD4 cells also activated the Act-1 pathway in epithelial cells to maintain barrier integrity (Lee et al., 2015) owing to the upregulation of MUC-2 production and strengthening of TJs attachments (Whibley and Gaffen, 2015; Lee et al., 2015). Additionally, CBM 588 does not ameliorate the colitis induced by clindamycin by using anti-IL-17A antibody (Figures 6A and 6B). IL-1β, TNF-α, and COX-2 RNA expressions were upregulated with anti-IL-17 antibody in CBM 588-treated mice, whereas IL-6 RNA expression was unaffected. Hence, the results suggested that IL-17 produced by γδ T cells and CD4 cell play an important role in protecting the colon from inflammation damage. Taken together, this study indicates that potential protective effects of CBM 588 on the intestinal barrier can be elucidated using an antibiotic-induced colitis model in ICR mice. CBM 588 upregulated the expression of IL-17-producing γδT cells and CD4 cells. Previous study identified three major RORgt + populations (γδT cells, CD4 cells, and ILC3s) in the colon after DSS treatment, and intracellular staining for IL-17A and IL-22 revealed that γδT cells were the major source of IL-17A in the cLP after DSS-induced injury, with more than 30% of cells expressing the cytokine and very few IL-22-producing γδT cells. In contrast to γδT cells, CD4 T cells only had a minor contribution to IL-17 and IL-22. Very few ILC3 cells were positive for IL-17A (Lee et al., 2015). Our results show that CBM 588 administration results in elevation of γδT cells and CD4 cells in cLP of mice and also upregulates IL-17A-producing γδT cells and CD4 cells in cLP. This helps preserve the integrity of antibiotic-damaged epithelial surfaces through the upregulation of TJs as well as mucin production.

CBM 588 Changes Gut Microbiome Metabolic Profiles to Protect the Gut Epithelial Barrier

Next, to elucidate the impact of CBM 588 on the underlying epithelial barrier protective mechanism against antibiotic damage, we investigated gut metabolic alterations by the resident microbiome. Phylogenetic Investigation of Communities by Reconstruction of Unobserved States (PICRUSt) was used to obtain relative Kyoto Encyclopedia of Genes and Genomes (KEGG) pathway abundance information derived from metagenomics data (Langille et al., 2013) (Figures 7A and 7B). We found that the activities of detailed metabolic pathways showed considerable variation. The combination group had a metabolic pathway activity similar to that of the clindamycin administration group. On the other hand, the combination group had higher relative activity compared with the clindamycin administration group, especially for "starch and sucrose metabolism" and "fructose and mannose metabolism" under carbohydrate

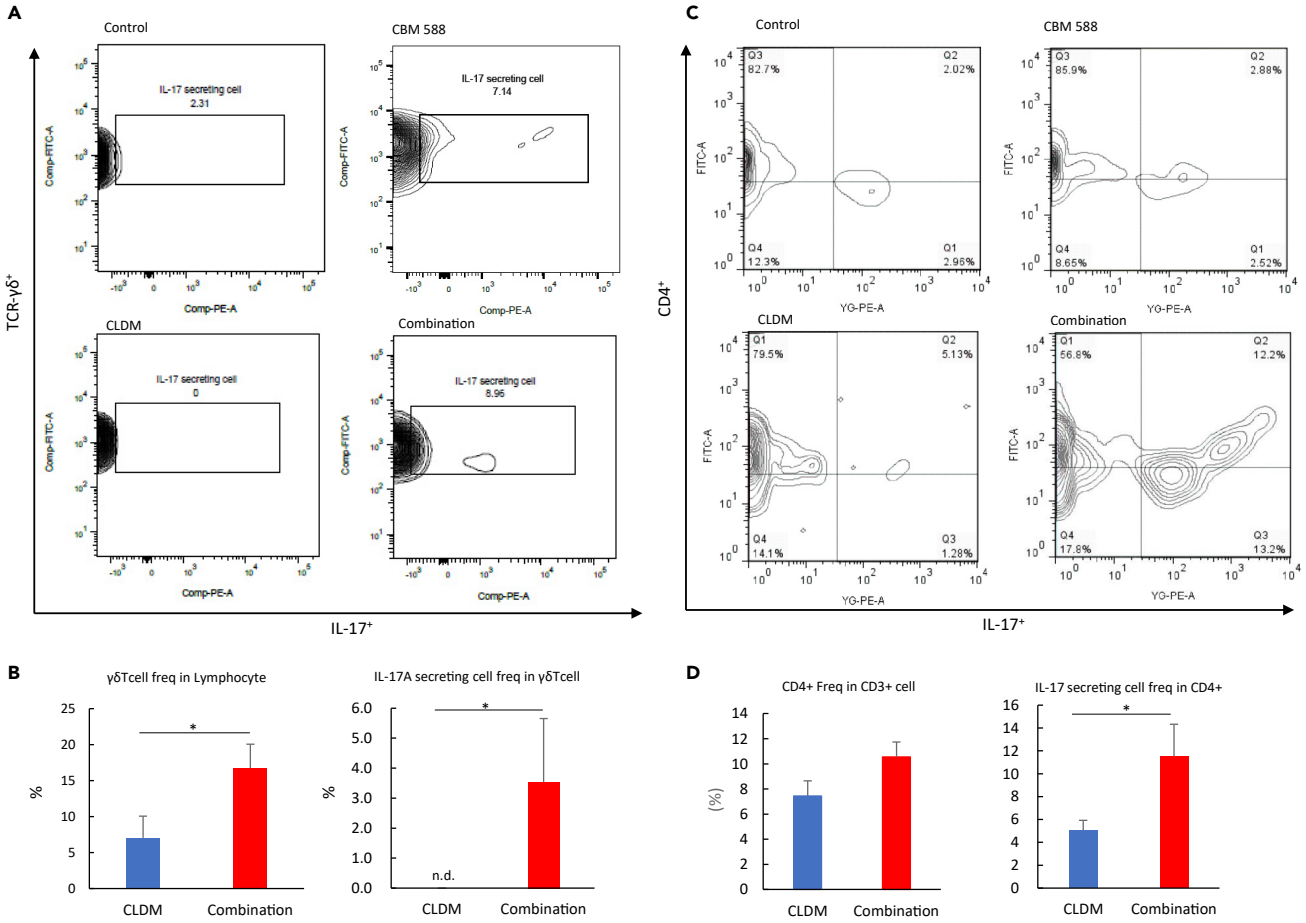

Figure 5. CBM 588 Upregulates IL-17A-producing γδT Cells and CD4 Cells

(A) Representative flow cytometry plots of γδT cells identified, and IL-17A-producing γδT cell expression among lymphocytes in colonic lamina propria (cLP) in the control group (Control), CBM 588 administration group (CBM 588), clindamycin administration group (CLDM), and combination group (Combination).

(B) Percentage of γδT cells in lymphocytes of cLP for the clindamycin administration group (CLDM) and combination group (left). Percentage of IL-17A secreting γδT cells among γδT cells in cLP cells (right).

(C) Representative flow cytometry plots of CD4 cells identified, and IL-17A-producing CD4 cell expression among lymphocytes in cLP in the control group (Control), CBM 588 administration group (CBM 588), clindamycin administration group (CLDM), and combination group (Combination).

(D) Percentage of CD4 cells in lymphocytes of cLP for the clindamycin administration group (CLDM) and combination group (left). Percentage of IL-17A secreting CD4 cells among CD3 cells in cLP cells (right).

All values, except Figures 5A and 5C, are mean ± SEM (n = 5–10). Statistical analysis of the quantitative multiple group comparisons was performed using a one-way analysis of variance followed by Tukey's test, *p < 0.05, n.d., not detected.

metabolism (Figure 7C). Certain bacteria of the intestinal flora are beneficial for gut health. Apart from immunomodulating capacities, these bacteria can also improve mucosal barrier integrity (Madsen et al., 2001). Hence, microbiome changes during CBM 588 treatment may contribute to attenuation of colon epithelial damages. Antibiotic-induced alteration of the mucous layer can lead to breaches in the epithelial barrier by specific bacteria, resulting in immune responses leading to chronic inflammation (Hagihara et al., 2018). Considering the increased abundance, only in the combination group, of bacterial species such as *Bifidobacterium*, *Lactobacillus,* and *Lactococcus,* that can use starch, sucrose, fructose, and mannose as energy sources, it appears that CBM 588 indirectly enhanced starch, sucrose, fructose, and mannose metabolism to produce glucose. Since mucin is an important source of carbohydrates for commensal bacteria, gut mucosal microbiome in inflamed regions can shift toward bacteria that metabolize "starch, sucrose, fructose and mannose" to maintain fixed amounts of energy production through the activation of carbohydrate metabolism (Kamada et al., 2013). Therefore, we believe that CBM 588 caused gut microbiome functional shifts toward increased carbohydrate metabolism through gut microbiome alternations.

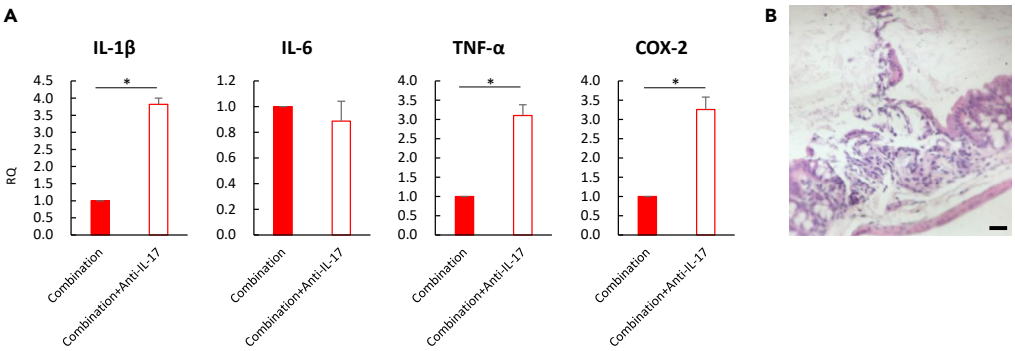

Figure 6. Anti-IL-17 Antibodies Reduced CBM 588 Effects on Intestinal Barrier Function

(A) The relative RNA expression levels of genes encoding IL-1β, IL-6, TNF-α, and COX-2 in colon tissue of mice detected at day 8 by qPCR. Expression of target genes was analyzed by the ΔΔCt method. Relative RNA expression levels of each target gene in mice treated with combination (clindamycin + CBM 588) + Anti-IL-17 antibodies were normalized to the combination group (represented as RQ).

(B) Hematoxylin and eosin (H&E) staining of colons at day 8 revealed superficial epithelial necrosis and the presence of inflammatory cells only in mice treated with combination (clindamycin + CBM 588) + Anti-IL-17 antibodies (magnification, 4× and the scale bar represents 150 μm).

All values are mean ± SEM (n = 5–10). Statistical analysis of the quantitative multiple group comparisons was performed using a one-way analysis of variance followed by Tukey's test, *p < 0.05, n.d., not detected.

In addition, we detected various metabolites in feces produced by the resident microbiome. Short-chain fatty acids (SCFAs) are the end products of microbial fermentation of non-digestible carbohydrates and have been reported to increase mucous secretion (Cummings and Macfarlane, 1991; Shimotoyodome et al., 2000). SCFAs are absorbed by the distal ileum and colon and are important sources of nutrition for epithelial cells (Cummings and Macfarlane, 1991; D'Argenio and Mazzacca, 1999) to promote mucosal restitution, induce differentiation, and inhibit inflammation (D'Argenio and Mazzacca, 1999; Awad et al., 1995). Organic acids in feces at day 4 and day 8 are shown in Figure 7D. Acetate concentration was decreased in the combination group, compared with the clindamycin administration group. Additionally, n-butyrate was seen only in the control group and CBM 588 administration group at day 4 but was found in all groups at day 8. The combination group showed a similar n-butyrate concentration as the clindamycin administration group. However, the combination group showed a higher ratio of n-butyrate/lactate than the clindamycin administration group at day 8 (Figure 7E). These results suggest that CBM 588 enhances the efficiency of lactate use for the production of butyrate, which is an anti-inflammatory SCFA that contributes to colon health and promotes the synthesis of mucin (Brown et al., 2011). Taken together, our results suggest that dysbiosis caused by antibiotics affects gut metabolite production in the resident microbiome. However, CBM 588 enhances carbohydrate metabolites and the production efficiency of n-butyrate, thus protecting the colon epithelial barrier, along with mucin production. Additionally, CBM 588 enhanced "lipid metabolism," "arachidonic acid metabolism," and "α-linoleic acid metabolism" pathways (Figure 7F). These results suggest that gut microbiome function shifts toward the production of prostaglandins and specialized pro-resolving lipid mediators (SPMs), including protectin D_1 and resolvin E, to counteract colon mucosa inflammation (Srivastava et al., 1982).

CBM 588 Promotes the Production of Anti-inflammatory Lipokines (Palmitoleic Acid), Prostaglandins Metabolites (15d-PGJ_2), and Specialized Pro-resolving Lipid Mediators (Protectin D_1) in Mouse Colon Tissue

Colon metabolites are the end products of cellular regulatory processes and have a strong correlation to phenotype. Levels of metabolites are also a predictor of a biological system's response to genetic and/or environmental changes. Since we found gut metabolic profile changes in lipid metabolites by the resident microbiome, we hypothesized that host colon tissue metabolic profiles would also change along with gut microbiome alternations. The PCA score plots for the control group and each treatment group are shown in Figure 8A. Samples clustered according to the treatment status of the mice ($p < 0.05$). The clindamycin administration group clustered separately ($p < 0.05$) from the CBM 588 administration group and combination group at day 4 but not at day 8 (Figures S5 and S6). As shown in Figure 8B, a heatmap was generated

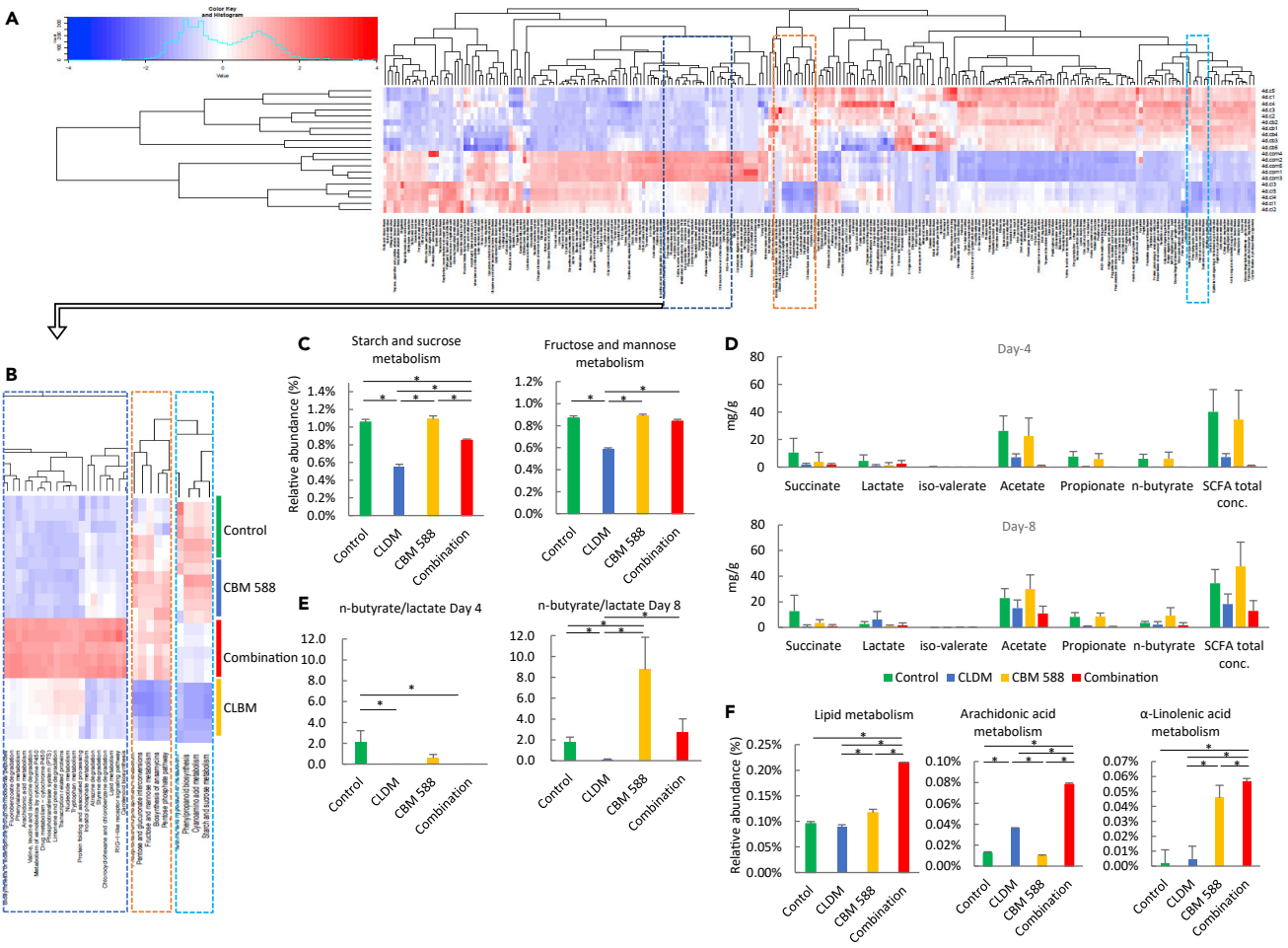

Figure 7. CBM 588 Changes Gut Microbiome Metabolic Profiles to Protect the Gut Epithelial Barrier

(A) Heatmaps, generated by hierarchical clustering, of selected colon metabolites at day 4, were significant between the control, clindamycin, and/or CBM 588 administration groups by Kruskal-Wallis test. An FDR p value < 0.05 was considered statistically significant, and the Benjamini-Hochberg method was used to calculate FDR p value.

(B) Expansion sites derived from Figure 7A.

(C) Comparison of the relative abundance of "starch and sucrose metabolism" and "fructose and mannose metabolism" in individual groups.

(D) The concentration of SCFAs in fecal samples. These fecal samples were taken at day 4 and day 8.

(E) The ratio of n-butyrate/lactate among all groups at day 4 and day 8.

(F) Comparison of the relative abundance of "lipid metabolism," "arachidonic acid metabolism," and "α-linoleic acid metabolism" in individual groups.

All values are mean ± SEM (n = 5–10). Statistical analysis of the quantitative multiple group comparisons was performed using a one-way analysis of variance followed by Tukey's test, *p < 0.05.

by hierarchical Pearson clustering of metabolites of colon tissue. The results showed a significant difference between the control group, clindamycin administration group, CBM 588 administration group, and combination group ($p < 0.05$) for 18 significant metabolites. Palmitic acid (C_{16}) and palmitoleic acid (C_{16}, ω-7), the monounsaturated fatty acid of palmitic acid that is classified as a lipokine, showed a higher concentration in the CBM 588 administration groups than in the clindamycin administration group and control group. Previous studies have revealed that palmitoleic acid suppresses inflammatory cytokine production and attenuates inflammation in metabolically active tissues (Cao et al., 2008; Chan et al., 2015). Additionally, it reverses macrophage polarization through the activation of AMP-activated protein kinase via peroxisome proliferator-activated receptor γ (PPARγ) activation (Chan et al., 2015). Previous study revealed that many intestinal bacteria can produce palmitic acid (Nagatake and Kunisawa, 2019). Bacteria-derived sphingolipids, which are endogenously produced from palmitic acid by serine-palmitoyl transferase, can act as signaling molecules to modulate host immune responses in the gut (Hosomi et al., 2019). Then, some kinds of gut commensal bacteria in the *Bacteroidetes* phylum produce sphingolipids through

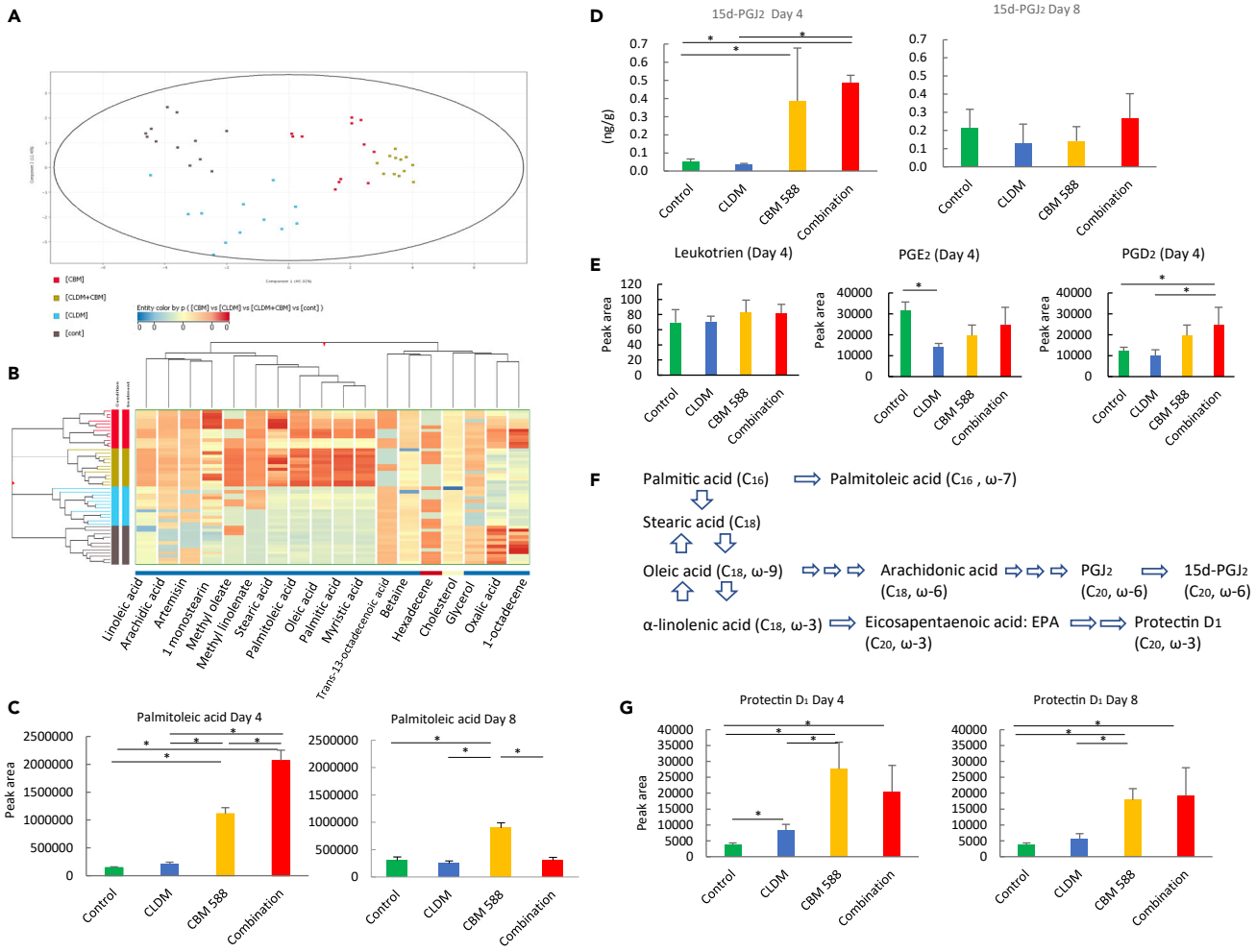

Figure 8. CBM 588 Promotes the Production of Several Anti-inflammatory Compounds in Mouse Colon Tissue

(A) PCA analysis representation of major sources of metabolite variability in the colon at day 4. Data points represent colon samples from three independent experiments (biological replicates; n = 5) injected randomly into the GC-MS.

(B) Heatmaps of selected colon metabolites, generated by hierarchical clustering, were significant between the control, clindamycin, and/or CBM 588 administration groups by Kruskal-Wallis test. An FDR p value < 0.05 was considered statistically significant, and the Benjamini-Hochberg method was used to calculate FDR p value.

(C) The peak height comparison of palmitoleic acid at day 4 and day 8 in each group.

(D) The concentration of 15d-PGJ_2 at day 4 and day 8.

(E) The peak height comparison of leukotriene, PGE_2, and PGD_2 at day 4. These results are represented with the mean ± SEM (n = 5).

(F) Featured metabolic pathway from palmitic acid to palmitoleic acid, 15d-PGJ_2, and Protectin D_1.

(G) The peak height comparison of protectin D_1 at day 4 and day 8.

These results are represented with the mean ± SEM (n = 5–10). *p < 0.05. Statistical analysis of the quantitative multiple group comparisons was performed using a one-way analysis of variance followed by Tukey's test, *p < 0.05.

bacterial serine-palmitoyl transferase. Hence, our metabolic profile analysis suggests that CBM 588 enhances palmitoleic acid production to reduce colon inflammation (Figure 8C).

Additionally, stearic acid (C_{18}) and oleic acid (C_{18}, ω-9) production were also enhanced in the CBM 588 administration groups (Figure 8B). We observed changes in COX-2 RNA expression in colon tissue, and gut residual microbiome enhanced arachidonic acid metabolism in addition to α-linoleic acid metabolism in CBM 588 administration groups (Figure 7F). Therefore, we hypothesized that CBM 588 enhanced the production of other anti-inflammatory lipid metabolites in colon tissue, since several members of the cyclopentenone family of prostaglandins and SPMs possess anti-inflammatory properties (Straus and Glass, 2001; Gobbetti et al., 2017). Consequently, we found higher concentrations of

15-deoxy-$\Delta^{12,14}$-prostaglandin (PG) J_2 (15d-PGJ_2) in colon tissue for the CBM 588 administration groups (Figure 8D). PGJ_2 is formed through dehydration within the cyclopentenone ring of the endogenous PGD_2. PGJ_2 is then further metabolized to yield D_{12}-PGJ_2 and 15d-PGJ_2. 15d-PGJ_2 is a high-affinity ligand for PPARγ. Various PPARγ ligands have been reported to possess anti-inflammatory properties *in vitro* (Jiang et al., 1998). It is possible that PPARγ trans-represses the expression of pro-inflammatory mediators at the transcriptional level by inhibiting NF-kB, STAT-1, and activator protein-1 (AP-1) signaling (Ricote et al., 1998). Previous studies have revealed that 15d-PGJ_2 inhibits chemokine expression and attenuates IκBα phosphorylation and nucleus translocation of NF-κB through a PPARγ-independent mechanism (Lu et al., 2013). 15d-PGJ2 is also known to have a potent suppressive effect on inflammatory responses via the Akt and NF-κB pathways, independent of PPARγ activation (Jung et al., 2009), in addition to attenuating the development of colon injury due to dinitrobenzene sulfonic acid in the IBD rat model (Cuzzocrea et al., 2003). In our study, arachidonic acid metabolism, especially 15d-PGJ_2, was upregulated (Figure 8D), whereas COX-2 RNA expression in colon tissue was reduced by CBM 588 (Figure 3D). Our results looked like contraindicated. However, COX-1 and COX-2 can produce PGD_2, which is the parent compound of 15d-PGJ_2, from arachidonic acid (Bie et al., 2018), and we admitted enhanced PGD_2 production in the combination group than in the clindamycin administration group (Figures 8E and 8F). On the other hand, PGE_2, metabolites by COX-2 from arachidonic acid, was decreased in the clindamycin administration group. Hence, our study suggests that CBM 588 enhances 15d-PGJ_2 production in colon tissue to suppress gut inflammation (Figure 8D).

Since we found that gut metabolites enhanced "α-linoleic acid metabolism" after CBM 588 administration (Figure 7F), we hypothesized that CBM 588 also enhances the production of other anti-inflammatory metabolites derived from α-linoleic acid in colon tissue. Accumulating evidence has shown ω3 lipid metabolites to be potent anti-inflammatory lipid mediators, such as protectin D_1 and resolvin E, which have been identified as new SPMs important in intestinal protection (Gobbetti et al., 2017). The resolution of inflammation is an active process with a mechanism partly linked to decreased leukocyte-endothelial interaction and reduced granulocyte trafficking by SPM that limits the host response within the affected tissue. Failure of effective resolution may lead to tissue injury (Gobbetti et al., 2017; Goto et al., 2015). In this study, CBM 588 enhanced protectin D_1 levels in colon tissue (Figure 8G) at day 4 and day 8. These results demonstrate that many types of metabolites with anti-inflammatory effects in host colon tissue, such as palmitoleic acid, 15d-PGJ_2, and protectin D_1, have enhanced production under CBM 588 treatment in an antibiotic-induced colitis model. This is the first study to show that probiotics enhance anti-inflammatory lipokines, PGs metabolites, and SPMs, to protect colon tissues from epithelial damage.

DISCUSSION

The intestinal epithelium is a critical barrier for protection against potential harmful microbiota or pathogens (Peterson and Artis, 2014). The epithelial barrier can be damaged with antibiotics, and CBM 588, used as a probiotic in Japan, has been shown to protect the epithelial barrier (Hagihara et al., 2018). However, the mechanism of protection is not entirely clear. Here we demonstrate that CBM 588 indirectly induces the differentiation of lymphocytes to IL-17A-producing γδT cells and IL-17A-producing CD4 cells in cLP to repair the damaged epithelium. Additionally, many types of metabolites with anti-inflammatory effects in host colon tissue, such as palmitoleic acid, 15d-PGJ_2, and protectin D_1, have enhanced production under CBM 588 treatment in an antibiotic-induced colitis model.

Similar to previous work, our studies have revealed that antibiotics induce gut dysbiosis and colitis (Lichtman et al., 2016). Clindamycin administration resulted in a dramatic reduction in gut microbiome diversity, and it seemed as if CBM 588 did not affect the gut microbiome composition at a phylum level. However, similar to a previous *in vivo* study (Hagihara et al., 2018), CBM 588 administration changed the gut microbiome at the genus level and increased the abundance of *Bifidobacterium*, *Lactobacillus*, and *Lactococcus* species. We therefore hypothesized that CBM 588 would impact many host physiological processes to maintain gut homeostasis. During antibiotic-induced dysbiosis, CBM 588 has been found to modulate inflammatory cytokines in colon tissue and exhibit a colitis-preventing effect through induction of TGF-β_1 in experimental DSS-induced acute colitis models (Kashiwagi et al., 2015; Hayashi et al., 2013). Consistent with these reports, this study showed that CBM 588 administration enhanced TGF-β_1 expression and reduced inflammatory cytokines, including IL-1β, IL-6, IFN-γ, COX-2, and TNF-α, while increasing IL-10 expression levels in colon tissue. Other studies have revealed that the TGF-β_1 pathway regulates inflammatory cytokine production as well as promotes the production of IL-10 (Hayashi et al., 2013). Therefore, our

data suggest that the anti-inflammatory effect of CBM 588 against clindamycin-induced colitis is associated with a TGF-β_1-dependent reduction of inflammatory cytokine expression and an increase in anti-inflammatory cytokines.

To further characterize the protective effects of CBM 588 on the epithelial barrier in antibiotic-induced colitis, we investigated RNA and protein expression levels of TJs and mucin-producing protein and found that CBM 588 upregulated expression levels of MUC-2 and tight junction complex proteins, whereas clindamycin downregulated these same proteins. Several investigations have found impaired TJ complexity and the downregulation of TJs in UC, which could be a mechanism responsible for intestinal barrier dysfunction (Pastorelli et al., 2013; Perse and Cerar, 2012). Another study showed that, after acute intestinal injury, intestinal-protective IL-17A could regulate TJs to limit excessive permeability and maintain barrier integrity (Lee et al., 2015; Benakis et al., 2016; Maxwell et al., 2015). Our results showed that CBM 588 induced an elevation of IL-17A protein expression in colon tissue. Previous study identified that γδT cells were the major source of IL-17A in cLP after DSS-induced injury, with more than 30% of cells expressing the cytokine. In contrast to γδT cells, CD4 cells only had a minor contribution to IL-17A and very few ILC3 cells were positive for IL-17A (Lee et al., 2015). Not surprisingly, we found an increase in γδT cells and IL-17A-producing γδT cells in the combination mice group, whereas no IL-17A-producing γδT cells were detected in the clindamycin administration group. Previous study suggested that TGF-β_1 signals are necessary for IL-17A production in γδ T cell (Shibata et al., 2011; Do et al., 2010). And, then, IL-6 need to enhance L-17A expression of γδ T cell, while we admitted the reduction of IL-6 RNA expression in colon tissue in combination group. However, *Clostridium*, *Bifidobacterium*, *Lactobacillus*, and *Lactococcus*, which are capable of microbial isoprenoid biosynthesis, have previously been found to induce the differentiation of lymphocytes to γδT cells and Th17 cells to protect colon epithelial cells (Roselli et al., 2009; Eberl et al., 2003; Yu et al., 2019; Veldhoen et al., 2006). IL-17A produced by γδT cells and CD4 cells also activated the Act-1 pathway in epithelial cells to maintain barrier integrity (Lee et al., 2015). Additionally, *Lactobacillus* can upregulate the expression of TJs and prevent the destruction of epithelial barrier function (Qin et al., 2009). Additionally, CBM 588 does not ameliorate the colitis induced by clindamycin by using anti-IL-17A antibody. Therefore, we hypothesized that IL-17A-producing γδT cells and CD4 cells may be involved in the CBM 588 protective mechanism for the colon mucosa, and TGF-β_1, *Bifidobacterium*, *Lactobacillus*, and *Lactococcus*, induced by CBM 588, play a key role in the enhanced expression of IL-17-producing γδ T cells and IL-17-producing CD4 cells in cLP to protect colon epithelial cells. Our results reveal a potent intestinal epithelial barrier protective mechanism whereby CBM 588 preserves the integrity of antibiotic-damaged epithelial surfaces.

Next, we investigated gut metabolic alterations by the resident microbiome and found CBM 588 enhanced "starch and sucrose metabolism" and "fructose and mannose metabolism." Because we observed an increased abundance in bacterial species that use starch, sucrose, fructose, and mannose as energy sources, such as *Bifidobacterium*, *Lactobacillus*, and *Lactococcus*, in our CBM 588 administration groups, we believed this microbiome change could contribute to attenuation of colon epithelial damages. This result has also been seen in our previous study (Hagihara et al., 2018). Mucin is an important source of carbohydrates for commensal bacteria. Additionally, SCFA in feces produced by the resident microbiome is an end product of microbial fermentation of non-digestible carbohydrates and has been reported to increase mucous secretion (Cummings and Macfarlane, 1991; Shimotoyodome et al., 2000). Gut mucosal microbiome in inflamed regions can shift its composition toward bacteria that metabolize starch, sucrose, fructose, and mannose, to maintain fixed amounts of energy production through the activation of carbohydrate metabolism (Kamada et al., 2013). In our study, the combination group decreased the concentration of SCFA compared with the CBM 588 administration group, whereas CB increased in gut compared with day 0. CBM 588 produced SCFA in our previous *in vivo* study using the same dosing schedule as in this study, whereas clindamycin was admitted in fecal sample at day 8 as more than 2 μg/g (Hagihara et al., 2018). Hence, we speculate the reason is that antibiotics killed many SCFA-producing bacteria in the digestive tract and the situation led to the reduction of SCFA production in clindamycin administration groups. Besides, we found that CBM 588 administration resulted in a higher ratio of n-butyric acid/lactic acid among all groups at day 8. Taken together, these results indicate that dysbiosis caused by antibiotics affected gut metabolites within the microbiome. However, CBM 588 enhanced carbohydrate metabolite production and SCFA production to protect the colon epithelial barrier. CBM 588 also enhanced the production efficiency of n-butyrate to protect the colon epithelial barrier through mucin production, as we found that MUC-2 expression levels were enhanced with CBM 588 administration. These results support

the hypothesis that CBM 588 contributes to increased carbohydrate metabolism, which aids in repairing the mucosal layer of the gastrointestinal tract.

We also found enhanced lipid metabolism, arachidonic acid metabolism, and α-linoleic acid metabolism pathways in the residual gut microbiome. These results imply that the gut microbiome is shifted toward the production of monounsaturated fatty acids, PGs, and SPMs, including protectin D_1 and resolvin E, to counteract the inflammation of colon mucosa (Srivastava et al., 1982). It is known that, in addition to mammalian cells, intestinal commensal bacteria also metabolize lipids and have a unique degradation pathway that yields unique metabolites. Therefore, the type of lipid produced is dependent on intestinal microbiota, which may be a critical determinant in the regulation of inflammatory responses (Gobbetti et al., 2017). Colon metabolites are the end products of cellular regulatory processes and correlate strongly with phenotype. Therefore, we hypothesized that CBM 588 enhances the production of anti-inflammatory metabolites in colon tissue. Consequently, palmitoleic acid (C_{16}, ω-7), which is classified as a lipokine and suppresses cytokine production (Cao et al., 2008; Chan et al., 2015) and macrophage polarization through the activation of AMP-activated protein kinase (Chan et al., 2015), showed a higher concentration in the CBM 588 administration groups. Additionally, we found upregulation of 15d-PGJ_2 and protectin D_1 in colon tissue in the CBM 588 administration groups. Lipid metabolites in host colon tissue that have potent anti-inflammatory effects, such as palmitoleic acid, 15d-PGJ_2, and protectin D_1, showed enhanced production with CBM 588 treatment under antibiotic-induced dysbiosis. This is the first study to show that probiotics change metabolic function in the residual gut microbiome and host colon tissue, resulting in enhanced anti-inflammatory lipokine, PG metabolites, and SPM production, which protects against colon epithelial damage. These findings suggest that the use of CBM 588, or probiotic treatment enhanced with *Bifidobacterium*, *Lactobacillus,* and *Lactococcus*, could be a potential therapeutic strategy in the control of intestinal inflammatory diseases.

In conclusion, this is the first report that CBM 588 enhances gut epithelial barrier function in mice with antibiotic-induced dysbiosis by expansion of IL-17A-producing γδT cells. Additionally, gut metabolic profiles were found to produce anti-inflammatory substances, such as palmitoleic acid, 15d-PGJ_2, and procaine D_1, and commensal metabolic alterations occurred between the host and gut microbiome. Our results will provide insight into the development of new probiotic treatments.

Limitations of the Study

Our study revealed some new insights for the mechanisms to show anti-inflammatory effects and epithelial protection effects with CBM 588. However, there are some limitations. First, in microbiome analysis, it was difficult to know the exact number of total bacteria. This issue made it difficult to know if the changes of relative abundances represent an increase in these bacteria or merely a shift in hierarchy. Hence, we compared relative abundances of specific bacterial species not only for clindamycin administration group and combination group data, but also for control and CBM 588 administration group data. Since the microbiome study results revealed that CBM 588 treatment did not affect gut microbiome α-diversity and β-diversity, relative abundances results will answer several differences derived from increasing bacteria or merely a shift in hierarchy. Consequently, we thought *Bifidobacterium* and *Lactococcus* were increased in the combination group, because they were increased in the CBM 588 administration group, compared with the control group. On the other hand, *Lactobacillus* was hierarchy increased in the combination group, because *Lactobacillus* did not increase in the CBM 588 administration group . Second, γδ T cells are more abundant in the intraepithelial region than in cLP, suggesting that it would be worth investigating the effect of CBM 588 on intraepithelial γδ T cells. However, previous study provides evidences that γδT cell populations in cLP are readily able to produce IL-17A protein upon activation and that these innate T lymphocytes are the early source of tissue-protective IL-17A during gut epithelial injury (Lee et al., 2015). Hence, we evaluated lymphocytes in cLP. Third, since we did not evaluate specific mechanism with knockout mice, we cannot conclude a definitive pathway. Additional study with IL-17A knockout mice could answer the research question stringently. However, previous study revealed that CBM 588 enhanced TGF-$β_1$ expression of dendritic cell (Kashiwagi et al., 2015), and *Bifidobacterium*, *Lactobacillus*, and *Lactococcus* have previously been found to induce the differentiation of lymphocytes to γδT cell and Th17 cells to protect colon epithelial cells (Roselli et al., 2009; Eberl et al., 2003; Yu et al., 2019; Veldhoen et al., 2006). Therefore, we speculate that TGF-$β_1$, *Bifidobacterium*, *Lactobacillus*, and *Lactococcus*, induced by CBM 588, play a key role in the enhanced expression of IL-17-producing γδ T cells and CD4 in cLP to protect colon epithelial cells. Also, detailed study is needed to determine the most important metabolite and its mechanism.

However, as we mentioned, each metabolite has been revealed to have anti-inflammatory effect in colon and they are related to the activation of PPARγ to show the effects. Hence, we speculate that PPARγ can play an important role, but further study needs to clear which metabolites have bigger impacts to show the effect.

METHODS

All methods can be found in the accompanying Transparent Methods supplemental file.

SUPPLEMENTAL INFORMATION

Supplemental Information can be found online at https://doi.org/10.1016/j.isci.2019.100772.

ACKNOWLEDGMENTS

This study was supported by Miyarisan Pharmaceutical Co., Ltd., which provided the CBM 588 powder. We also thank the Division of Laboratory Animal Research (Aichi Medical University) for providing the facilities for performing the animal experiments and the Division of Advanced Research Promotion (Aichi Medical University) for technical instructions and assistance. Finally, we would like to thank Editage (www.editage.com) for English language editing.

AUTHOR CONTRIBUTIONS

M.H., R.Y., A.M., K.O., M.T., and H.M. contributed to the study design. M.H. performed and/or contributed critically to all experiments and analyzed the data. In some experiments, Y.K. assisted in performing r16S sequencing. T.A., K.F., K.M., N.Y., S.O., T.O., and S.T. assisted in performing mass-spectrum assays. K.I. assisted in conducting flow cytometry analysis. T.M. and T.N. assisted in conducting tissue evaluation. M.H. and H.M. wrote the manuscript. All authors read and approved the manuscript.

DECLARATION OF INTERESTS

The authors declare no competing financial interests.

Received: June 30, 2019
Revised: October 13, 2019
Accepted: December 10, 2019
Published: January 24, 2020

REFERENCES

Alvarez, C.S., Badia, J., Bosch, M., Giménez, R., and Baldomà, L. (2016). Outer membrane vesicles and soluble factors released by probiotic *Escherichia coli* nissle 1917 and commensal ECOR63 enhance barrier function by regulating expression of tight junction proteins in intestinal epithelial cells. Front. Microbiol. *7*, 1981.

Atarashi, K., Tanoue, T., Shima, T., Imaoka, A., Kuwahara, T., Momose, Y., Cheng, G., Yamasaki, S., Saito, T., Ohba, Y., et al. (2011). Induction of colonic regulatory T cells by indigenous *Clostridium* species. Science *331*, 337–341.

Awad, A.B., Kamei, A., Horvath, P.J., and Fink, C.S. (1995). Prostaglandin synthesis in human cancer cells: influence of fatty acids and butyrate. Prostaglandins Leukot. Essent. Fatty Acids *53*, 87–93.

Bartlett, J.G. (2002). Clinical practice. Antibiotic-associated diarrhea. N. Engl. J. Med. *346*, 334–339.

Benakis, C., Brea, D., Caballero, S., Faraco, G., Moore, J., Murphy, M., Sita, G., Racchumi, G., Ling, L., Pamer, E.G., et al. (2016). Commensal microbiota affects ischemic stroke outcome by regulating intestinal γδ T cells. Nat. Med. *22*, 516–523.

Bie, Q., Dong, H., Jin, C., Zhang, H., and Zhang, B. (2018). 15d-PGJ2 is a new hope for controlling tumor growth. Am. J. Transl. Res. *10*, 648–658.

Brown, C.T., Davis-Richardson, A.G., Giongo, A., Gano, K.A., Crabb, D.B., Mukherjee, N., Casella, G., Drew, J.C., Ilonen, J., Knip, M., et al. (2011). Gut microbiome metagenomics analysis suggests a functional model for the development of autoimmunity for type 1 diabetes. PLoS One *6*, e25792.

Cao, H., Gerhold, K., Mayers, J.R., Wiest, M.M., Watkins, S.M., and Hotamisligil, G.S. (2008). Identification of a lipokine, a lipid hormone linking adipose tissue to systemic metabolism. Cell *134*, 933–944.

Chan, K.L., Pillon, N.J., Sivaloganathan, D.M., Costford, S.R., Liu, Z., Theret, M., Chazaud, B., and Klip, A. (2015). Palmitoleate reverses high fat-induced proinflammatory macrophage polarization via AMP-activated protein kinase (AMPK). J. Biol. Chem. *290*, 16979–16988.

Cummings, J.H., and Macfarlane, G.T. (1991). The control and consequences of bacterial fermentation in the human colon. J. Appl. Bacteriol. *70*, 443–459.

Cuzzocrea, S., Ianaro, A., Wayman, N.S., Mazzon, E., Pisano, B., Dugo, L., Serraino, I., Di Paola, R., Chatterjee, P.K., Di Rosa, M., et al. (2003). The cyclopentenone prostaglandin 15-deoxy-D12,14-PGJ2 attenuates the development of colon injury caused by dinitrobenzene sulphonic acid in the rat. Br. J. Pharmacol. *138*, 678–688.

D'Argenio, G., and Mazzacca, G. (1999). Short-chain fatty acid in the human colon. Relation to inflammatory bowel diseases and colon cancer. Adv. Exp. Med. Biol. *472*, 149–158.

Deitch, E.A. (2002). Bacterial translocation or lymphatic drainage of toxic products from the gut: what is important in human beings? Surgery *131*, 241–244.

Dnucan, S.H., Hold, G.L., Barcenilla, A., Stewart, C.S., and Flint, H.J. (2002). *Roseburia intestinalis* sp. nov., a novel saccharolytic, butyrate-producing bacterium from human faeces. Int. J. Syst. Evol. Microbiol. *52*, 1615–1620.

Do, J.S., Fink, P.J., Li, L., Spolski, R., Robinson, J., Leonard, W.J., Letterio, J.J., and Min, B. (2010). Cutting edge: spontaneous development of IL-17-producing γδ T cells in the thymus occurs via a TGF-β1-dependent mechanism. J. Immunol. *184*, 1675–1679.

Eberl, M., Hintz, M., Reichenberg, A., Kollas, A.K., Wiesner, J., and Jomaa, H. (2003). Microbial isoprenoid biosynthesis and human gammadelta T cell activation. FEBS Lett. *544*, 4–10.

Ekmekciu, I., von Klitzing, E., Fiebiger, U., Neumann, C., Bacher, P., Scheffold, A., Bereswill, S., and Heimesaat, M.M. (2017). The probiotic compound VSL modulates mucosal, peripheral, and systemic immunity following murine broad-spectrum antibiotic treatment. Front. Cell Infect. Microbiol. *7*, 167.

Elinav, E., Strowig, T., Kau, A.L., Henao-Mejia, J., Thaiss, C.A., Booth, C.J., Peaper, D.R., Bertin, J., Eisenbarth, S.C., Gordon, J.I., et al. (2011). NLRP6 inflammasome regulates colonic microbial ecology and risk for colitis. Cell *145*, 745–757.

Ferrer, M., Martins dos Santos, V.A., Ott, S.J., and Moya, A. (2014). Gut microbiota disturbance during antibiotic therapy: a multi-omic approach. Gut Microbes *5*, 64–70.

Garrett, W.S., Lord, G.M., Punit, S., Lugo-Villarino, G., Mazmanian, S.K., Ito, S., Glickman, J.N., and Glimcher, L.H. (2007). Communicable ulcerative colitis induced by T-bet deficiency in the innate immune system. Cell *131*, 33–45.

Gobbetti, T., Dalli, J., Colas, R.A., Federici Canova, D., Aursnes, M., Bonnet, D., Alric, L., Vergnolle, N., Deraison, C., Hansen, T.V., et al. (2017). Protectin D1n-3 DPA and resolvin D5n-3 DPA are effectors of intestinal protection. Proc. Natl. Acad. Sci. U S A *114*, 3963.

Goto, T., Kim, Y.I., Furuzono, T., Takahashi, N., Yamakuni, K., Yang, H.E., Li, Y., Ohue, R., Nomura, W., Sugawara, T., et al. (2015). 10-oxo-12(Z)-octadecenoic acid, a linoleic acid metabolite produced by gut lactic acid bacteria, potently activates PPARγ and stimulates adipogenesis. Biochem. Biophys. Res. Commun. *459*, 597–603.

Hagihara, M., Yamashita, R., Matsumoto, A., Mori, T., Kuroki, Y., Kudo, H., Oka, K., Takahashi, M., Nonogaki, T., Yamagishi, Y., et al. (2018). The impact of *Clostridium butyricum* MIYAIRI 588 on the murine gut microbiome and colonic tissue. Anaerobe *54*, 8–18.

Hayashi, A., Sato, T., Kamada, N., Mikami, Y., Matsuoka, K., Hisamatsu, T., Hibi, T., Roers, A., Yagita, H., Ohteki, T., et al. (2013). A single strain of *Clostridium butyricum* induces intestinal IL-10-producing macrophages to suppress acute experimental colitis in mice. Cell Host Microbe *13*, 711–722.

Hempel, S., Newberry, S.J., Maher, A.R., Wang, Z., Miles, J.N., Shanman, R., Johnsen, B., and Shekelle, P.G. (2012). Probiotics for the prevention and treatment of antibiotic-associated diarrhea: a systematic review and meta-analysis. JAMA *307*, 1959–1969.

Hooper, L.V., Littman, D.R., and Macpherson, A.J. (2012). Interactions between the microbiota and the immune system. Science *336*, 1268–1273.

Hosomi, K., Kiyono, H., and Kunisawa, J. (2019). Fatty acid metabolism in the host and commensal bacteria for the control of intestinal immune responses and diseases. Gut Microbes, 1–9.

Huang, X., Zou, Y., Lian, L., Wu, X., He, X., He, X., Wu, X., Huang, Y., and Lan, P. (2013). Changes of T cells and cytokines TGF-β1 and IL-10 in mice during liver metastasis of colon carcinoma: implications for liver anti-tumor immunity. J. Gastrointest. Surg. *17*, 1283–1291.

Ivanov, I.I., Atarashi, K., Manel, N., Brodie, E.L., Shima, T., Karaoz, U., Wei, D., Goldfarb, K.C., Santee, C.A., Lynch, S.V., et al. (2009). Induction of intestinal Th17 cells by segmented filamentous bacteria. Cell *139*, 485–498.

Jiang, C., Ting, A.T., and Seed, B. (1998). PPAR-gamma agonists inhibit production of monocyte inflammatory cytokines. Nature *391*, 82–86.

Johnson-Henry, K.C., Donato, K.A., Shen-Tu, G., Gordanpour, M., and Sherman, P.M. (2008). *Lactobacillus rhamnosus* strain GG prevents enterohemorrhagic Escherichia coli O157: H7-induced changes in epithelial barrier function. Infect. Immun. *76*, 1340–1348.

Jung, W.K., Park, I.S., Park, S.J., Yea, S.S., Choi, Y.H., Oh, S., Park, S.G., and Choi, I.W. (2009). The 15-deoxy-Delta-12,14-prostaglandin J2 inhibits LPS-stimulated AKT and NF-kappaB activation and suppresses interleukin-6 in osteoblast-like cells MC3T3E-1. Life Sci. *85*, 46–53.

Kamada, N., Chen, G.Y., Inohara, N., and Núñez, G. (2013). Control of pathogens and pathobionts by the gut microbiota. Nat. Immunol. *14*, 685–690.

Kashiwagi, I., Morita, R., Schichita, T., Komai, K., Saek,i, K., Matsumoto, M., Takeda, K., Nomura, M., Hayashi, A., Kanai, T., et al. (2015). Smad2 and Smad3 inversely regulate TGF-β autoinduction in *Clostridium butyricum*-activated dendritic cells. Immunity *43*, 65–79.

Langille, M.G., Zaneveld, J., Caporaso, J.G., McDonald, D., Knights, D., Reyes, J.A., Clemente, J.C., Burkepile, D.E., Vega Thurber, R.L., Knight, R., et al. (2013). Predictive functional profiling of microbial communities using 16S rRNA marker gene sequences. Nat. Biotechnol. *31*, 814–821.

Lee, J.S., Tato, C.M., Joyce-Shaikh, B., Gulen, M.F., Cayatte, C., Chen, Y., Blumenschein, W.M., Judo, M., Ayanoglu, G., McClanahan, T.K., et al. (2015). Interleukin-23-independent IL-17 production regulates intestinal epithelial permeability. Immunity *43*, 727–738.

Lichtman, J.S., Ferreyra, J.A., Ng, K.M., Smits, S.A., Sonnenburg, J.L., and Elias, J.E. (2016). Host-microbiota interactions in the pathogenesis of antibiotic-associated diseases. Cell Rep. *14*, 1049–1061.

Lu, Y., Zhou, Q., Zhong, F., Guo, S., Hao, X., Li, C., Wang, W., and Chen, N. (2013). 15-Deoxy-Delta(12,14)-prostaglandin J(2) modulates lipopolysaccharide-induced chemokine expression by blocking nuclear factor-kappaB activation via peroxisome proliferator activated receptor-gamma-independent mechanism in renal tubular epithelial cells. Nephron Exp. Nephrol. *123*, 1–10.

Madsen, K., Cornish, A., Soper, P., McKaigney, C., Jijon, H., Yachimec, C., Doyle, J., Jewell, L., and De Simone, C. (2001). Probiotic bacteria enhance murine and human intestinal epithelial barrier function. Gastroenterology *121*, 580–591.

Martini, E., Krug, S.M., Siegmund, B., Neurath, M.F., and Becker, C. (2017). Mend your fences, the epithelial barrier and its relationship with mucosal immunity in inflammatory bowel disease. Cell Mol. Gastroenterol. Hepatol. *4*, 33–46.

Maxwell, J.R., Zhang, Y., Brown, W.A., Smith, C.L., Byrne, F.R., Fiorino, M., Stevens, E., Bigler, J., Davis, J.A., Rottman, J.B., et al. (2015). Differential roles for interleukin-23 and interleukin-17 in intestinal immunoregulation. Immunity *43*, 739–750.

McFarland, L.V. (2014). Use of probiotics to correct dysbiosis of normal microbiota following disease or disruptive events: a systematic review. BMJ Open *4*, e005047.

Nagatake, T., and Kunisawa, J. (2019). Emerging roles of metabolites of ω3 and ω6 essential fatty acids in the control of intestinal inflammation. Int. Immunol. *31*, 569–577.

Ni, Y., Teng, T., Li, R., Simonyi, A., Sun, G.Y., and Lee, J.C. (2017). TNFα alters occludin and cerebral endothelial permeability: role of p38MAPK. PLoS One *12*, e0170346.

Pastorelli, L., Salvo, C.D., Mercado, J.R., Vecchi, M., and Pizarro, T.T. (2013). Central role of the gut epithelial barrier in the pathogenesis of chronic intestinal inflammation: lessons learned from animal models and human genetics. Front. Immunol. *4*, 280.

Paul, S., Shilpi, and Lal, G. (2015). Role of gamma-delta (gammadelta) T cells in autoimmunity. J. Leukoc. Biol. *97*, 259–271.

Perse, M., and Cerar, A. (2012). Dextran sodium sulphate colitis mouse model: traps and tricks. J. Biomed. Biotechnol. *2012*, 718617.

Peterson, L.W., and Artis, D. (2014). Intestinal epithelial cells: regulators of barrier function and immune homeostasis. Nat. Rev. Immunol. *14*, 141–153.

Qin, H., Zhang, Z., Hang, X., and Jiang, Y. (2009). *L. plantarum* prevents enteroinvasive *Escherichia coli*-induced tight junction proteins changes in intestinal epithelial cells. BMC Microbiol. *9*, 63–71.

Resta-Lenert, S., and Barrett, K.E. (2006). Probiotics and commensals reverse TNF-a and IFN-r induced dysfunction in human intestinal epithelial cells. Gastroenterology *130*, 731–746.

Ricote, M., Li, A.C., Willson, T.M., Kelly, C.J., and Glass, C.K. (1998). The peroxisome proliferator activated receptor-gamma is a negative regulator of macrophage activation. Nature *391*, 79–82.

Roselli, M., Finamore, A., Nuccitelli, S., Carnevali, P., Brigidi, P., Vitali, B., Nobili, F., Rami, R.,

Garaguso, I., and Mengheri, E. (2009). Prevention of TNBS-induced colitis by different Lactobacillus and Bifidobacterium strains is associated with an expansion of gammadeltaT and regulatory T cells of intestinal intraepithelial lymphocytes. Inflamm. Bowel Dis. *15*, 1526–1536.

Seki, H., Shiohara, M., Matsumura, T., Miyagawa, N., Tanaka, M., Komiyama, A., and Kurata, S. (2003). Prevention of antibiotic-associated diarrhea in children by *Clostridium butyricum* MIYAIRI. Pediatr. Int. *45*, 86–90.

Shibata, K., Yamada, H., Sato, T., Dejima, T., Nakamura, M., Ikawa, T., Hara, H., Yamasaki, S., Kageyama, R., Iwakura, Y., et al. (2011). Notch-Hes1 pathway is required for the development of IL-17-producing γδ T cells. Blood *118*, 586–593.

Shimotoyodome, A., Meguro, S., Hase, T., Tokimitsu, I., and Sakata, T. (2000). Short chain fatty acids but not lactate or succinate stimulate mucus release in the rat colon. Comp. Biochem. Physiol. A Mol. Integr. Physiol. *125*, 525–531.

Srivastava, K.C., Awasthi, K.K., Lindegård, P., and Tiwari, K.P. (1982). Effect of some saturated and unsaturated fatty acids on prostaglandin biosynthesis in washed human blood platelets from (1-14 C) arachidonic acid. Prostaglandins Leukot. Med. *8*, 219–237.

Straus, D.S., and Glass, C.K. (2001). Cyclopentenone prostaglandins: new insights on biological activities and cellular targets. Med. Res. Rev. *21*, 185–210.

Veldhoen, M., Hocking, R.J., Atkins, C.J., Locksley, R.M., and Stockinger, B. (2006). TGFbeta in the context of an inflammatory cytokine milieu supports de novo differentiation of IL-17-producing T cells. Immunity *24*, 179–189.

Vijay-Kumar, M., Aitken, J.D., Carvalho, F.A., Cullender, T.C., Mwangi, S., Srinivasan, S., Sitaraman, S.V., Knight, R., Ley, R.E., and Gewirtz, A.T. (2010). Metabolic syndrome and altered gut microbiota in mice lacking Tolllike receptor 5. Science *328*, 228–231.

Whibley, N., and Gaffen, S.L. (2015). Gut-busters: IL-17 Ain't Afraid of No IL-23. Immunity *43*, 620–622.

Wiström, J., Norrby, S.R., Myhre, E.B., Eriksson, S., Granström, G., Lagergren, L., Englund, G., Nord, C.E., and Svenungsson, B. (2001). Frequency of antibiotic-associated diarrhoea in 2462 antibiotic-treated hospitalized patients: a prospective study. J. Antimicrob. Chemother. *47*, 43–50.

Willemsen, L.E., Koetsier, M.A., van Deventer, S.J., and van Tol, E.A. (2003). Short chain fatty acids stimulate epithelial mucin 2 expression through differential effects on prostaglandin E(1) and E(2) production by intestinal myofibroblasts. Gut *52*, 1442–1447.

Yu, R., Zuo, F., Ma, H., and Chen, S. (2019). Exopolysaccharide-producing bifidobacterium adolescentis strains with similar adhesion property induce differential regulation of inflammatory immune response in Treg/Th17 axis of DSS-colitis mice. Nutrients *11*, E782.

iScience, Volume *23*

Supplemental Information

Clostridium butyricum Modulates the Microbiome to Protect Intestinal Barrier Function in Mice with Antibiotic-Induced Dysbiosis

Mao Hagihara, Yasutoshi Kuroki, Tadashi Ariyoshi, Seiya Higashi, Kazuo Fukuda, Rieko Yamashita, Asami Matsumoto, Takeshi Mori, Kaoru Mimura, Naoko Yamaguchi, Shoshiro Okada, Tsunemasa Nonogaki, Tadashi Ogawa, Kenta Iwasaki, Susumu Tomono, Nobuhiro Asai, Yusuke Koizumi, Kentaro Oka, Yuka Yamagishi, Motomichi Takahashi, and Hiroshige Mikamo

Transparent Methods

Medicine. CBM 588 bacterial powder was used for all *in vivo* studies and was used at a concentration of $2.2*10^{10}$ cfu/g (Lot 61GT: MIYARISAN Pharmaceutical Co. Ltd.). Clindamycin for injections was purchased from Pfizer Japan Inc. Immediately before each *in vivo* experiment, CBM 588 powder was weighed and reconstituted with sterile water. Clindamycin was further diluted in appropriate diluents to achieve the desired concentration. Clindamycin solution was stored under refrigeration and discarded 12 h after reconstitution. Neutralizing antibody to IL-17A was generated at BD Biosciences.

Animals and housing. Pathogen-free, female ICR mice (9-10 weeks) weighing approximately 30 g were obtained from Charles River Laboratories Japan, Inc., (Yokohama, Japan). Mice were maintained and utilized under National Research Council recommendations, and were provided food and water *ad libitum*. The study was reviewed and approved by the ethics committee of the Aichi Medical University (2018-75).

Method of administration. Twenty female ICR mice were divided into the following four groups (n = 5): (i) control group, (ii) clindamycin single administration group, (iii) CBM 588 single administration group and (iv) combination group (CBM 588 + clindamycin). CBM 588 was administered by oral gavage at 500 mg/kg/day (3.4×10^8 cfu/kg/day). Clindamycin was also administered by oral gavage at 40 mg/kg/day. CBM 588 powder was dissolved into sterilized water, and the suspension was mixed and given to mice via sonde. For combination groups, CBM 588 and clindamycin were dissolved into sterilized water separately. Mice were given the suspension twice a day, at 10 a.m. and 4 p.m., using a half dose each time, over the course of 4 days. Anti-Mouse IL-17A (clone TC11-18H10) was dosed at 500 µg i.p. once at Day0.

Assessment of physiological condition. Weight loss and stool consistency were assessed daily to determine any possible physical changes. Body weight was recorded every other day. These data were reported as percentage of weight loss from initial body weight.

Histological examination. At Day 8, subsets of mice from each group were sacrificed to check histological changes in colon tissue. At the harvest, mice were euthanized by an overdose of CO_2 followed by cervical dislocation. Fixed sections of colonic tissues were embedded in paraffin. These tissues were then cut into 3-µm sections, and stained with

hematoxylin and eosin (H&E) for histological analysis via light microscopy. These samples were evaluated by a skilled pathologist, focusing on the following parameters associated with colitis: (1) neutrophil margination and tissue infiltration, (2) hemorrhagic congestion and edema of the mucosa, and (3) epithelial cell damage. A score of 0-3, denoting increasingly sever abnormality was assigned to each of these parameters and their combined scores graphed.

Analysis of intestinal permeability in mice. To determine *in vivo* intestinal permeability, mice were starved overnight, and then FITC-dextran (Sigma) was administered by oral gavage (44 mg/100 g body weight). After 4 hr, mice were anesthetized, blood was collected by cardiac puncture, and mice were sacrificed. Serum was separated from whole blood using BD Microtainer SST Tubes (BD), diluted with an equal volume of PBS (pH 7.4), and 100 µl of diluted serum was added to a 96-well microplate. The concentration of FITC in serum was determined by spectrophoto fluorometry, with an excitation of 485 nm and an emission wavelength of 528 nm, using serially diluted FITC-dextran as standard (Gupta et al., 2014).

Method of examining *C. butyricum* in feces. Day 0 indicates the day before the addition of medicine; medicine was given on days 2 and 4; examination was performed on days 2, 4 and 14 after termination (days 6, 8, and 18 from initial administration of medicine). On the selected days, at least 0.05 g feces were collected and put into a 0.45 ml transport medium. For determination of fecal *C. butyricum* concentrations, *C. butyricum* selective medium was used (Yamazaki, 1988). The fecal specimens were diluted between 10x and 100,000x. Specimens were placed in culture medium separately, smeared evenly, and cultured for 24 h. *C. butyricum* growth was then detected in culture medium. Viable count was calculated by counting the number of colonies growing on plates, and data are converted to equal numbers in per gram of feces. Additionally, we exposed 0.05 ml of undiluted fecal specimens to ethanol. The same process was performed with these samples to reveal the numbers of *C. butyricum* spores in feces. The testing detectable level is above 2.0 (log amount) per gram of feces.

DNA extraction. To characterize the microbiome composition in the colon, fecal samples from each mouse were analyzed by sequencing the 16S rRNA gene V3–V4 regions. DNA extraction and sequencing of 16S rRNA encoding gene amplicons was conducted as previously described (Hagihara et al., 2018). Briefly, fecal pellets were suspended in 10 mM Tris-HCl and 10 mM EDTA buffer (pH 8.0) and incubated with lysozyme

(Sigma, final concentration: 15 mg/mL) at 37˚C for 1 h. A purified achromopeptidase (Wako) was added (final concentration: 2,000 U/mL) and further incubated at 37˚C for another 30 min. SDS (final concentration: 1%) was then added to the cell suspension and mixed well. Subsequently, proteinase K (Merck) was added (final concentration: 1 mg/mL) to the suspension, and the mixture was incubated at 55˚C for 1 h. High-molecular-mass DNA was isolated and purified by phenol/chloroform extraction, ethanol, and finally polyethylene glycol precipitation.

Gut microbiome analysis. Meta 16S rRNA gene sequencing PCR was performed using Ex Taq Hot Start (TAKARA) and the Illumina forward primer 50-AATGATACGGCGACCACCGAGATCTACAC (adaptor sequence) +barcode (eight bases) + ACACTCTTTCCCTACACGACGCTCTTCCGATCT (sequence primer) + CCTACGGGNGGCWGCAG-30 (341F) and the Illumina reverse primer 50-CAAGCAGAAGACGGCATACGAGAT (adaptor sequence) + barcode (eight bases) + GTGACTGGAGTTCAGACGTGTGCTCTTCCGATCT (sequence primer) + GACTACHVGGGTATCTAATCC-30 (805R) to the hypervariable V3–V4 region of the 16Sr RNA gene. Amplicons generated from each sample were subsequently purified using SPRI select (Beckman Coulter). DNA was quantified using a Quantus Fluorometer and the QuantiFluor dsDNA System (Promega). Mixed samples were prepared by pooling approximately equal amounts of amplified DNA, and sequenced using MiSeq Reagent Kit V3 (600 cycle) and MiSeq sequencer (Illumina), according to the manufacturer's instructions.

The 16S rRNA sequence data generated by the MiSeq sequencer (Illumina) were processed by the quantitative insights into microbial ecology (QIIME 1.8.0) pipeline (Caporaso et al., 2010; Caporaso and Kuczynski et al., 2010). Sequences with an average quality value of < 20 were filtered out, and chimeric sequences were removed using USEARCH (Edgar, 2010). Sequences were clustered into operational taxonomic units (OTUs) based on 97% sequence similarity at the species level using UCLUST (Edgar, 2010) against Green genes database 13_8 (DeSantis et al., 2006). A representative sequence for each OTU was aligned with PyNAST (Caporaso et al., 2010). Bacterial taxonomy was assigned using UCLUST (Edgar, 2010). Genomic DNA from 20 Strain Even Mix Genomic Material (ATCC® MSA-1002™) was used in the study to evaluate data analysis procedures.

Alpha (α)-and beta (β)-diversity analysis. Within-community diversity (α-diversity) was calculated using QIIME. An α-rarefaction was generated using a Chao 1 estimator of

species richness with 10 sampling repetitions at each sampling depth (Chao, 1984). An even depth of ~3119 sequences per sample was used for calculation of richness and diversity indices. To compare microbial composition between samples, ß-diversity was measured by calculating the weighted unifrac distances using QIIME default scripts (Lozupone and Knight, 2005). Principal coordinate analysis (PCoA) was applied on the resulting distance matrices to generate two-dimensional plots. Each colored point represents a fecal sample obtained from one mouse coloring is according to different treatments (control, clindamycin administration group, CBM 588 administration group, and combination group). *p*-values were calculated using PERMANOVA. Samples clustered according to treatment status of the mice ($p < 0.05$).

Predictive functional profiling of gut microbial communities (PICRUSt). To gain more insight into the metagenomics-based function of the microbiome in each group of mice, the Phylogenetic Investigation of Communities by Reconstruction of Unobserved States (PICRUSt) v1.1.1 was used (Langille et al., 2013). PICRUSt was used to obtain relative Kyoto Encyclopedia of Genes and Genomes (KEGG) pathway abundance information derived from metagenomics data (Langille et al., 2013). The predicted data were collapsed into hierarchical categories (KEGG-Level-3), and the relative abundances of the gut metabolic functions were calculated and graphed using R software. We only focused on level 3 to investigate the impact of clindamycin and CBM 588 administrations on gut microbial functions. The heatmap was generated by hierarchical clustering of relative abundances of metabolic pathways with Z-score normalization. A Kruskal-Wallis test was employed for statistical analysis. The differentially expressed compounds with an FDR $p < 0.05$ were considered statistically significant, with the Benjamini-Hochberg method used to calculate the FDR *p* value.

Organic acids. At the end of the treatment period on day 4, and 4 days after CBM 588 and clindamycin treatment were discontinued (day 8), at least 0.3 g feces were collected from each mouse in the four groups. For determination of organic acids, 0.1 g of feces was placed in a 2.0 mL-tube with zirconia beads and suspended in MilliQ. Samples were heated at 85°C for 15 min, vortexed at 5 m/s for 45 s using FastPrep 24 (MP Biomedicals, CA, USA), and centrifuged at 15,350 × *g* for 10 min. The supernatant was filtrated with a 0.2 μm filter. Organic acids (acetate, propionate, n-butyrate, iso-valerate, succinate, lactate,) in feces were measured with high performance liquid chromatography (Prominence, SHIMADZU, Kyoto, Japan) using a post column reaction with a detector (CDD-10A, SHIMADZU, Kyoto, Japan), tandemly-arranged

two columns (Shim-pack SCR-102 (H), 300 mm × 8 mm ID, SHIMADZU, Kyoto, Japan), and a guard column (Shim-pack SCR-102 (H), 50 mm × 6 mm ID, SHIMADZU, Kyoto, Japan). The system was used with a mobile phase (5 mM p-toluenesulfonic acid) and a reaction solution (5 mM p-toluenesulfonic acid, 100 μM EDTA, and 20 mM Bis-Tris). The flow rate and oven temperature were 0.8 mL/min and 40°C, respectively. The detector cell temperature was kept at 48°C. Detection limits for acetic acid, propionic acid, butyric acid, iso-butyric acid, succinic acid, lactic acid, formic acid, valeric acid, and iso-valeric acid were 0.05, 0.05, 0.1, 0.1, 0.05, 0.05, 0.1, 0.1 and 0.1 mg/g, respectively.

RNA isolation and preparation of cDNA. To analyze the RNA expression of intracellular cytokines, total RNA was isolated by homogenizing mouse colons (30 mg) using the RNA isolation Kit (MACHEREY-NAGEL, Germany) in accordance with manufacturer's instructions. For preparation of complementary DNA (cDNA), Highcapacity RNA to cDNA kit (Thermofisher, USA) was used in accordance with manufacturer's instructions. Total RNA solution (9 μL) was added to 2*RT Buffer mix and 20*RT Enzyme Mix for a final volume of 20 μl. The mixture was incubated at 37°C for 60 minutes, and stopped by heating to 95°C for 5 minutes and holding at 4°C. For convenience, the incubation was performed in a thermal cycler. The cDNA was either immediately used in real-time PCR applications or placed for long-term storage in a freezer (−20°C).

Quantitative real-time PCR. Quantitative RT-PCR analysis was performed using the PowerUp™ SYBR™ Green PCR Master Mix (Applied Biosystems, USA) in accordance with the manufacturer's protocol. Briefly, PCR reactions were performed in a reaction mixture (10 μL) containing 2 μL of cDNA, 5 μL of PowerUp™ SYBR™ Green PCR Master Mix, 0.5 μL of 10 μM forward primer, 0.5 μL of 10 μM reverse primer, and 2 μL of nuclease-free water. The sequences of primers are summarized in Table S1. Amplification conditions were 2 min at 50°C, 2 min at 95°C, and 40 cycles of denaturation at 95°C for 15 s with annealing/extension at 60°C for 1 min, when Tm ≥ 60°C. Amplification conditions were 2 min at 50°C, 2 min at 95°C, with 40 cycles of denaturation at 95°C for 15 s, annealing at 60°C for 15 s min, and extension at 72°C for 1 min, when Tm < 60°C. For relative quantitation, we compared the amount of target normalized to an endogenous reference, ß-actin. The formula 2ΔΔCt represents the n-fold differential expression of a specific gene in a treated sample compared with the control, where Ct is the mean of threshold cycle, ΔCt is the difference in Ct values for

the target gene and the reference gene, ß-actin (in each sample), and ΔΔCt represents the difference between the Ct from the control and each datum. We validated this method by first comparing the standard curves of the reference and the target to show that the efficiencies were equal. Immediately after amplification, melt curve protocol was utilized to guarantee minimization in primer dimers and other non-specific products. Expression of target genes was analyzed by the ΔΔCt method. Relative RNA expression levels of each target gene were normalized to the control group (represented as RQ).

Cytokine studies. The colon tissue samples were homogenized in a RIPA buffer supplemented with protease inhibitors (Nacalai tesque). After sonication for 10 s, the suspension was centrifuged at 10,000 × g for 20 min at 4°C. Protein expression of interleukin-6, interleukin-17 and tumor necrosis factor-α (TNF-α) in the supernatants were measured by commercially available mouse cytokine enzyme-linked immunosorbent assay (ELISA) kits (R&D Systems, Minneapolis, MN). Protein expression of Mucine (MUC)-2 and Zonula occludens protein 1 (ZO-1) were also measured by commercially available mouse ELISA kits (Cusabio technology, USA and LSBio, USA). These procedures were performed according to the manufacturer's instructions.

Tissue sample preparation for mass spectrometry. The colon tissue samples were homogenized in a RIPA buffer supplemented with protease inhibitors (Nacalai tesque). After sonication for 10 s, the suspension was centrifuged at 10,000 × g for 20 min at 4°C. Frozen supernatants from the mouse colon samples (stored −80◦C) were thawed once to 0°C. Immediately after being thawed, a portion of the supernatant sample (100 µL) was added to a solution consisting of 400 µL of a mixture of chloroform/methanol (2:1, v/v), and the resulting mixture was vigorously agitated for 1 min. The mixture was then centrifuged at 20,000 x g for 10 min, and the organic phase was collected. The remaining precipitate and aqueous phase were then mixed with 400 L of chloroform, and the resulting mixture was centrifuged at 15,000 rpm for 10 min to give the organic phase. The combined organic phases were then evaporated to give the residues.

GC-MS. The Shimadzu QP2010 Ultra gas chromatograph system coupled with a mass spectrometer was applied for GC-MS data acquisition. GC-MS analysis was performed according to a previous study (Yamada et al., 2013). The system utilized a 30 m x 0.25 mm i.d. fused silica capillary column coated with 0.25 µm CP-SIL 8 CB low bleed

(Agilent). Injection volume: 1 μL, with splitless injector; carrier gas: Helium; the front inlet purge flow: 20 mL/min; initial temperature: 70 °C for 1 min, then raised to 280 °C at a rate of 6 °C/min, and maintained for 5 min at 280 °C. Injection temperature: 280 °C; transfer line temperature: 280 °C; ion source temperature: 250 °C. Electron impact mode energy: −70 eV; solvent delay: 366 s; full-scan mode range: 50~600 m/z; scan rate: 20 spectra per second. For sample pretreatment and derivatization, each evaporated sample derived from 100 μL of the tissue supernatant in a 1-mL EP tube. 100 μL THF was added to each of the dried samples and vortex-mixed for 2 min, and 50 μL BSTFA was added to the mixture and vortex-mixed for 2 min. The mixture was incubated at 60°C and derivatized for 30 min. After returning to ambient temperature, samples were prepared for GC/MS analysis.

Compound identification was performed by comparing the mass spectrum with a Fiehn metabolomics mass spectra library. Peaks with similarity index more than 60% were assigned compound names, while those having less than 60% similarity were listed as unknown metabolites. The chromatograms were subjected to noise reduction prior to peak area integration. Any known artificial peaks, such as peaks due to noise, column bleed and MSTFA derivatization procedure, were excluded from the data set. Integrated peak areas of multiple derivative peaks belonging to the same compound were summed and considered as a single compound. The relative peak area of each compound would be calculated as the response after the peak areas of compounds were integrated. Each sample was represented by a PCA score plots for the control and each treatment group, and the heatmap was generated by hierarchical Pearson clustering of metabolites of colon tissue. A Kruskal-Wallis test was employed for statistical analysis. The differentially expressed compounds with FDR $p < 0.05$ were considered statistically significant, with the Benjamini-Hochberg method used to calculate FDR p value. PCA and clustering was used to differentiate the samples and performed using the Mass Profiler Professional Version 14.9 (Agilent Technologies Inc.).

LC-MS/MS. Methyl acetate and ethyl acetate were purchased from Kanto Chemical (Tokyo, Japan). LC–MS grade formic acid, HPLC grade acetonitrile, methanol and distilled water were purchased from FUJIFILM Wako Pure Chemical Corporation (Osaka, Japan). Prostanoids used as standards were obtained from Cayman Chemical Company (Ann Arbor, MI, USA). For preparation of standards, standard stock solutions (1 mg/mL) of individual 15d-PGJ_2 were prepared in methyl acetate. The internal standard stock solutions (0.1 mg/mL) of 15d-PGJ_2-d_4 were also prepared in methyl acetate. Serial dilutions of standard stock solutions with methyl acetate were

performed for method validation.

The combined organic phases were then evaporated to dryness in vacuo to give the residues, which were individually dissolved in 100 L of acetonitrile. Aliquots (10 µL) of these stock solutions were analyzed with a previously described method (Tachi et al., 2014). In brief, 40 µL of prepared samples were spiked with 10 µL of the internal standard mixture containing 10 ng/mL 15d-PGJ_2-d_4 for calibration. Ethyl acetate (1 mL) was then added to the samples. The solution was shaken for 30 s and centrifuged for 2 min at 10,000 × g. The ethyl acetate phase containing the prostanoids was collected and dried with a centrifugal vacuum system. The residue was dissolved in 50 µL 25% methanol containing 0.1% formic acid, and then filtered with Millex®-HV (0.45 µm, Millipore Co., MA, USA). A 20 µL aliquot of the resulting sample was subjected to liquid chromatography-ion trap tandem mass spectrometry (LC-$ITMS^n$) analysis. To measure prostanoid concentration of the samples, the peak area ratio relative to the internal standard was calculated and determined from the corresponding calibration curve.

LC separation was performed at room temperature with an ACCELA HPLC system (Thermo Fisher Scientific, Waltham, MA, USA) equipped with a Synergi Hydro-RP column (150 × 2.0 mm i.d., 4.0 µm, Phenomenex, CA, USA). The mobile phases were 40% acetonitrile (A), and 100% methanol (B). The LC elution gradient employed was: 0 to 2.0 min 100% eluent A, 2.0 to 4.0 min eluent A decreased linearly to 50%, and then to 100% eluent B within 1.0 min. 100% Eluent B was held for 4.2 min. The eluent was then shifted back to 100% A, which was held for 3.7 min to equilibrate the column for the next sample. The flow rate was 0.2 mL/min. Mass spectrometric analysis was accomplished using an LTQ Velos (Thermo Fisher Scientific) equipped with a heated electrospray ionization source. The negative ion mode was chosen for prostanoid detection. The source voltage was set at 3 kV, while the capillary temperature was set at 350 °C and the tube lens offset was set at 15 V. The sheath gas flow rate was 35 (arbitrary units) and the auxiliary gas flow rate was 10 (arbitrary units). Full scan experiments were performed in the range of m/z 50–1000. Total microscans were set at 1, and the maximum injection time was set at 10 ms. Subsequent MS/MS experiments were performed in the range of m/z 70–600. The maximum injection time was set at 100 ms (Tachi et al., 2014).

UHPLC-Triple TOF/MS. The combined organic phases were then evaporated to dryness in vacuo to give the residues, which were individually dissolved in 100 µL of acetonitrile. UHPLC-Triple TOF/MS analyses were performed on a Shimadzu UHPLC

Nexera X2 system (Shimazu) using a CORTECS® C18 column (2.7 µm, 100 mm × 2.1 mm, Waters) and a Triple TOF 5600+ (SCIEX) with an electrospray ionization device running in the positive ion mode. The detector conditions were as follows: ionspray voltage at 5500 V, source temperature of 350◦C, ion source gas 1, 60 psi, ion source gas 2 60 psi, declustering potential, 80 V and collision energies of 45 V, collision energy spread, 15 V. Nitrogen was used as the collision gas. The protectin D_1 derivatives were detected using the MRM^{HR} mode. This strategy was designed to detect a specific product ion with an m/z 359.2223/45.0019 by protectin D_1. In terms of the mobile phases used for the UHPLC-Triple TOF/MS analyses, solvent A consisted of a 0.1% (v/v) solution of formic acid in water, whereas solvent B consisted of a 0.1% (v/v) solution of formic acid in acetonitrile. The protectin D_1 derivatives were eluted from the column using a linear gradient, which started at 80% solvent A and 20% solvent B, and progressed to 100% solvent B over a period of 10 min. The system was then eluted with 100% solvent B for 10 min before being returned to the initial conditions over a period of 10 min to allow for the equilibration of the column. The system was operated at a constant flow rate of 0.2 mL/min for all of the analyses. The raw data "mzXML" was used to convert to "abf " format with the ABF converter. The MS DIAL equipped with FiehnLib24 was used for raw peaks exaction, peak alignment, deconvolution analysis and identification.

Isolation of lymphocytes from colon tissue. To isolate colon lumina propria lymphocytes, large intestines was collected and opened longitudinally, washed to remove fecal content, and shaken in HBSS containing 1.5% fetal bovine serum (FBS) and 0.5 M EDTA for 20 min at 37°C. After removing epithelial cells and fat tissue, the intestines were cut into small pieces and incubated with HBSS containing 1.5% FBS and 1 mg/ml collagenase type IV (CLSS, WOR) for 1 h at 37°C in a shaking water bath. The digested tissues were processed through a 100 µm filter (pluriSelect, Germany) and resuspended in 5 ml of 40% Percoll (GE Healthcare) before overlay on 5 ml of 80% Percoll in a 15-ml Falcon tube. Percoll gradient separation was performed by centrifugation at 800 g for 20 min at 20°C. The interface cells were collected and used as LP lymphocytes.

Flow cytometry analysis. The collected cells were then resuspended in RPMI 1640 containing 10% FBS. For detection of IL-17, lymphocytes were stimulated for 4 h with 50 ng/mL PMA (Sigma) and 1 µg/mL ionomycin (Sigma). Cells were first stained for surface CD3, then fixed and permeabilized using a BD Cytofix/Cytoperm kit (554714,

BD Biosciences), and finally stained for intracellular IL-17. The following antibodies were used: FITC-labeled anti-CD4 cell (561535, BD Biosciences), Per-CP-labeled anti-CD3 Ab (561089, BD Biosciences), PE-labeled anti-CD8 Ab (561095, BD Biosciences), FITC-labeled anti-γδT cell receptor (11-5711-82, eBioscience), and PE-labeled anti-IL-17 Ab (559502, BD Biosciences). Flow cytometry was performed using FACSCant™ II (BD Biosciences) and data were analyzed with FlowJo software (TreeStar Inc).

Immunohistochemical staining to determine the IgA. We used immunohistochemistry to detect the protein expression of IgA in colon tissues. Strong IgA expression was not detected in all groups (Supplemental data 3). Formalin-fixed, paraffin-embedded colon tissue was analyzed using immunohistochemistry. The samples were deparaffinized and dehydrated. After the sections were subjected to antigen retrieval in an autoclave, immunohistochemical staining was performed by incubating the sections overnight with a mouse anti-IgA (α), Mouse, Goat-Poly antibody (Funakoshi, Japan). The sections were then incubated with an avidin-biotin complex reagent (VECTASTAIN Elite ABC Goat IgG Kit, Funakoshi). The sections were counterstained with hematoxylin, and immunoreactivity of the IgA proteins was assessed.

Statistics and analysis. For *C. butyricum* colony counts, all the data were presented as the mean ± SD. Unpaired *t*-tests were performed using JMP. $p < 0.05$ was the level of significance. For microbiome analysis, all data in bar graph or dot plot formats are expressed as mean ± SD. Differences were considered statistically significant at $p < 0.05$. For the microbiome data, Kruskal-Wallis analysis (non-parametric equivalent to ANOVA) was used to compare average proportions of each taxon level (phylum, class, order, family, and genus) in mouse fecal samples. Mann-Whitney U test was used to determine significant differences between each treatment group.

Supplemental Figure legends

Figure S1. Bacterial composition in different experimental groups at the species level, Related to Figure 2. 4d: sampling at day 4, 8d: sampling at day 8.

Figure S2. The relative RNA expression levels of genes encoding IL-1ß, IL-6, TNF-α, NF-κB, COX-2, INF-γ, IL-17A, TLR-2, HSP-70, TGF-ß1 and IL-10 in colon tissue of mice at Day 4, as detected by qPCR, Related to Figure 3.

Figure S3. Immunohistochemical staining to determine the IgA in colon tissues, Related to Figure 3. Upper: hematoxylin and eosin (H&E) staining of colons at Day 8 in all groups (Control group: Control, CBM 588 administration group: CBM 588, clindamycin administration group: CLDM, combination group: Combination) (magnification, 10X and the scale bar represents 150 μm). Low: immunohistochemical staining to determine the IgA in colon tissues of all groups (magnification, 20X and the scale bar represents 150 μm). Strong IgA expression was not detected in all groups. Formalin-fixed, paraffin-embedded colon tissue was analyzed using immunohistochemistry. The samples were deparaffinized and dehydrated.

Figure S4. (A) Representative flow cytometry plots of CD4 cells and CD8 cells identified among CD3 cells in colonic lamina propria (cLP) in the control group (Control), CBM 588 administration group (CBM 588), clindamycin administration group (CLDM), and combination group (Combination), Related to Figure 5.
(B) Percentage of CD3 cells among lymphocytes in cLP cells for the clindamycin administration group (CLDM) and combination group (left). Percentage of CD8 cells among CD3 cell in cLP cells for the clindamycin administration group (CLDM) and combination group (right), Related to Figure 5. Percentage of CD4-CD8- cells among CD3 cell in cLP cells for the clindamycin administration group (CLDM) and combination group (below). All values, except Figure 4A, are mean ± SEM (n = 5). Statistical analysis of the quantitative multiple group comparisons was performed using a one-way analysis of variance followed by Tukey's test, *$p < 0.05$, n.d., not detected.

Figure S5. Heat maps of selected colon metabolites at Day 8, generated by hierarchical clustering, were significant between the control, clindamycin, and /or CBM 588 administration groups by Kruskal-Wallis test, Related to Figure 7. An FDR p-value < 0.05 was considered statistically significant, and the Benjamini-Hochberg method was

used to calculate FDR p value. 8d: sampling at Day 8. Control group, CLDM administration group, CBM 588 administration group, and Combination group represent C1-5, cl1-5, cb1-5 and com1-5, respectively. Specific metabolic changes were not observed within each group.

Figure S6. PCA representation of major sources of metabolite variability in the colon at Day 8, Related to Figure 8. Data points represent colon samples from three independent experiments (biological replicates; n = 5) injected randomly into the GC-MS. Heat maps of selected colon metabolites, generated by hierarchical clustering, were significant between the control, clindamycin, and /or CBM 588 administration groups by Kruskal-Wallis test. An FDR p-value < 0.05 was considered statistically significant, and the Benjamini-Hochberg method was used to calculate the FDR p value.

Supplemental Figure 1

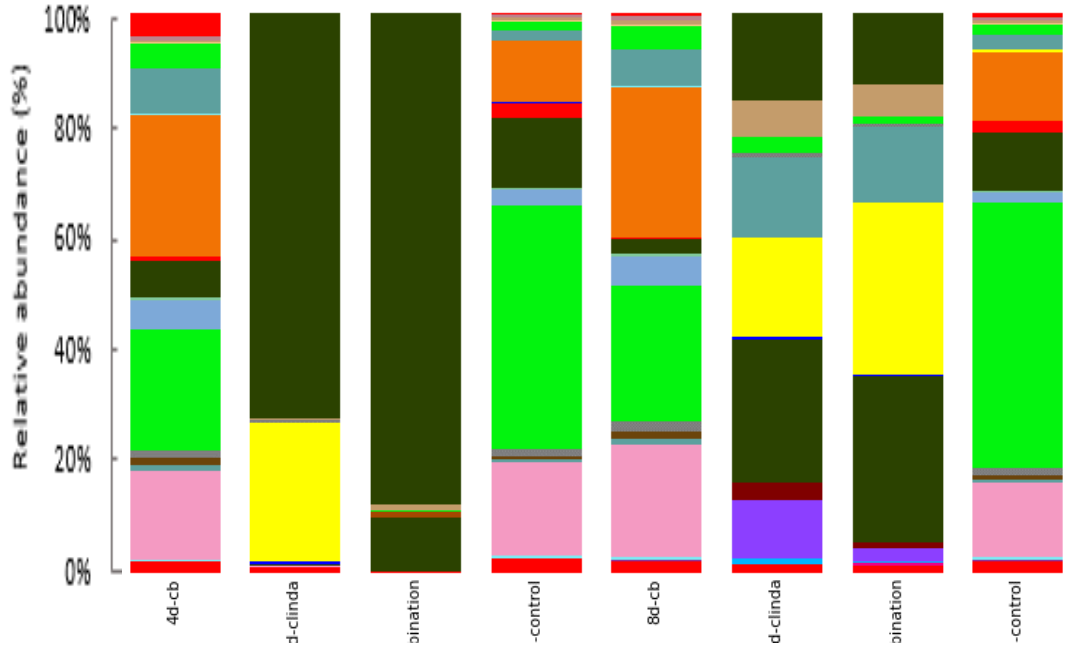

Supplemental Figure 2

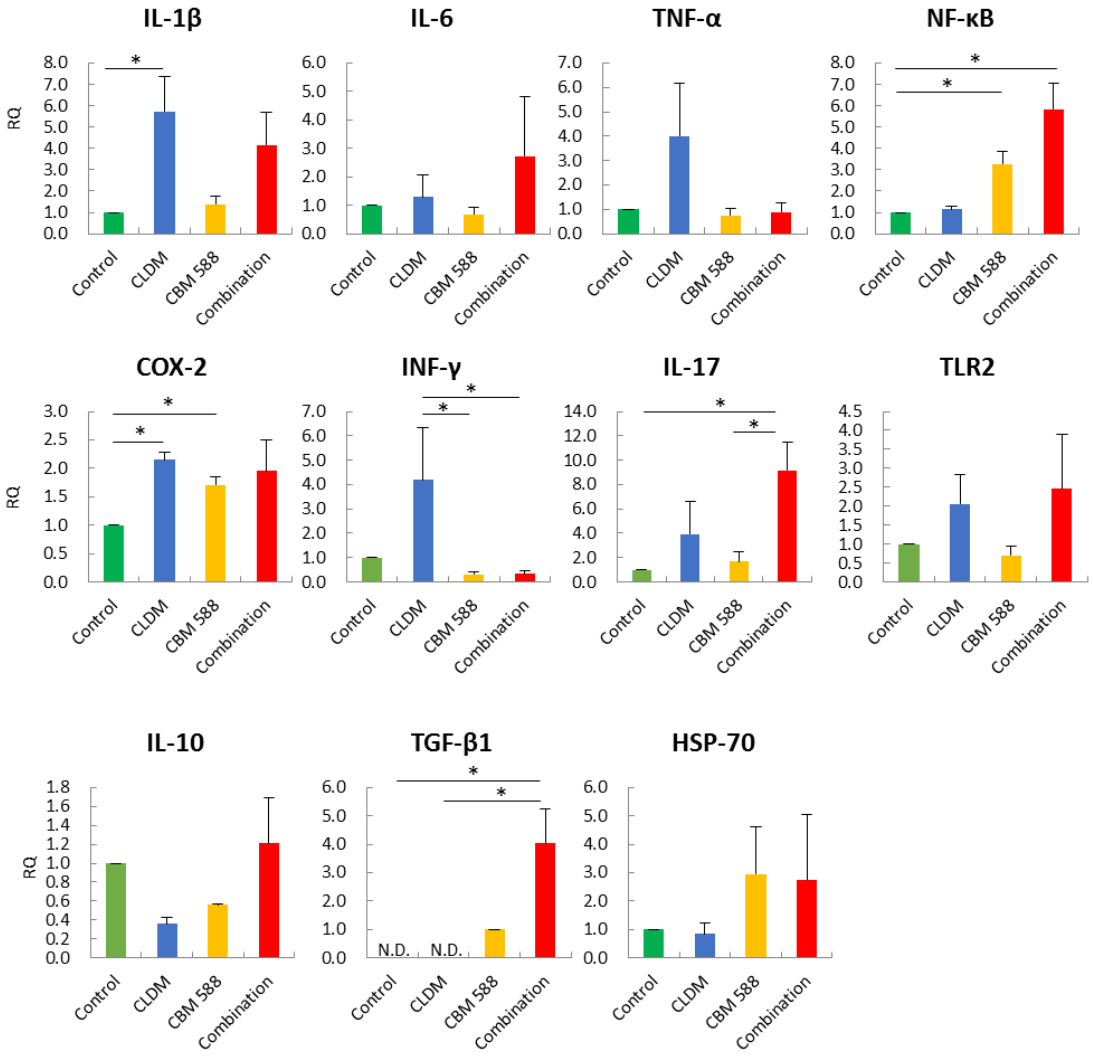

Supplemental Figure 3

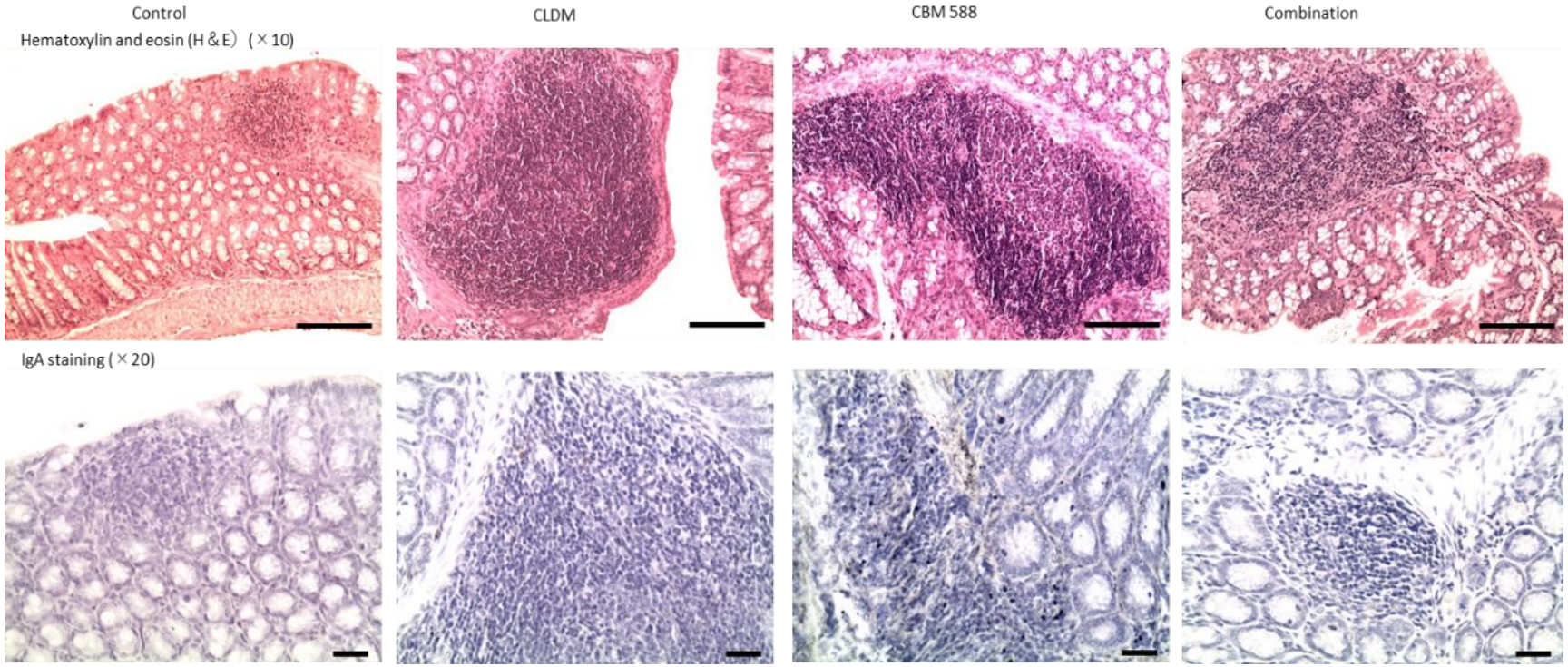

Supplemental Figure 4

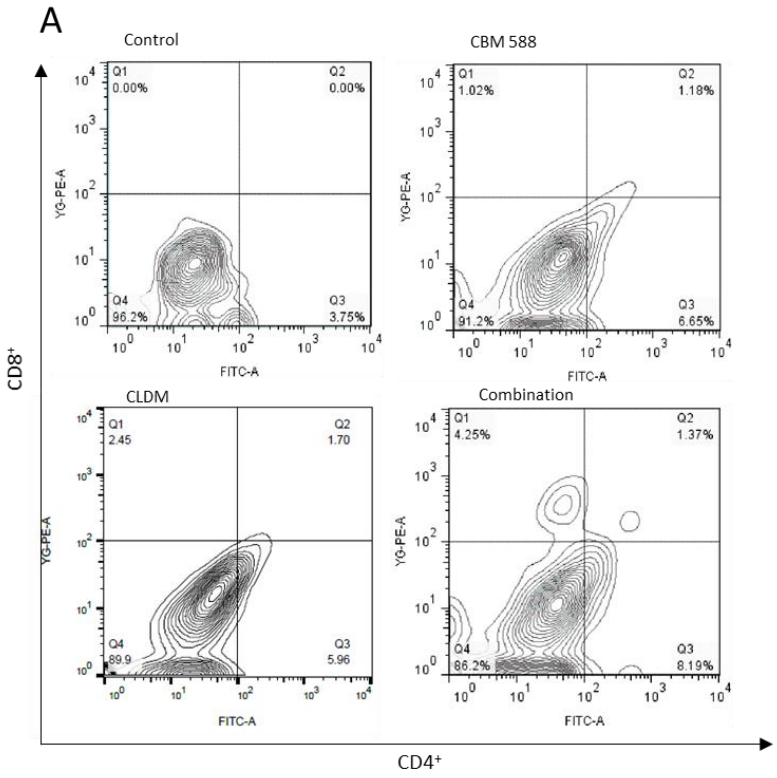

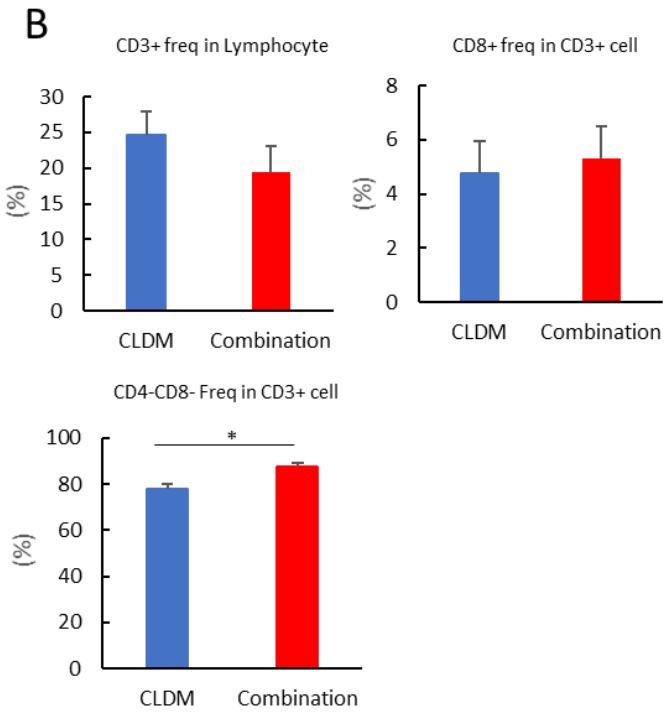

Supplemental Figure 5

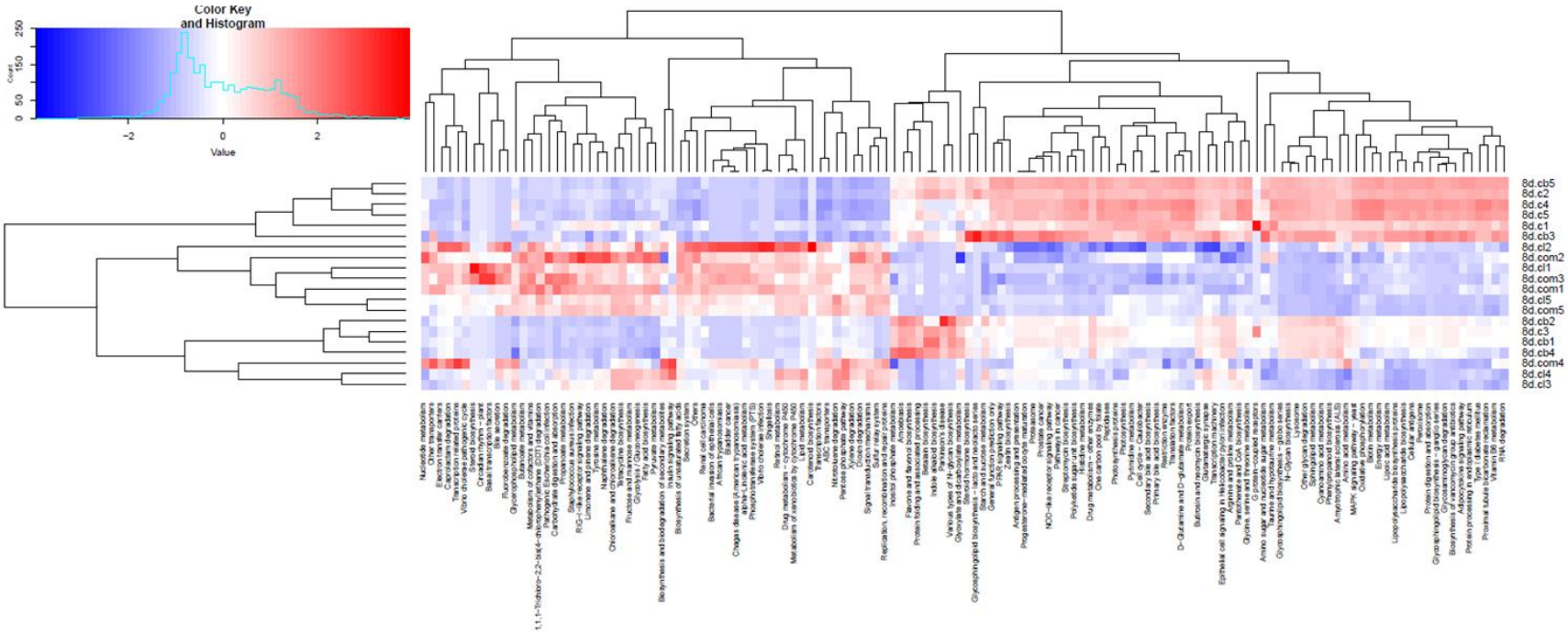

Supplemental Figure 6

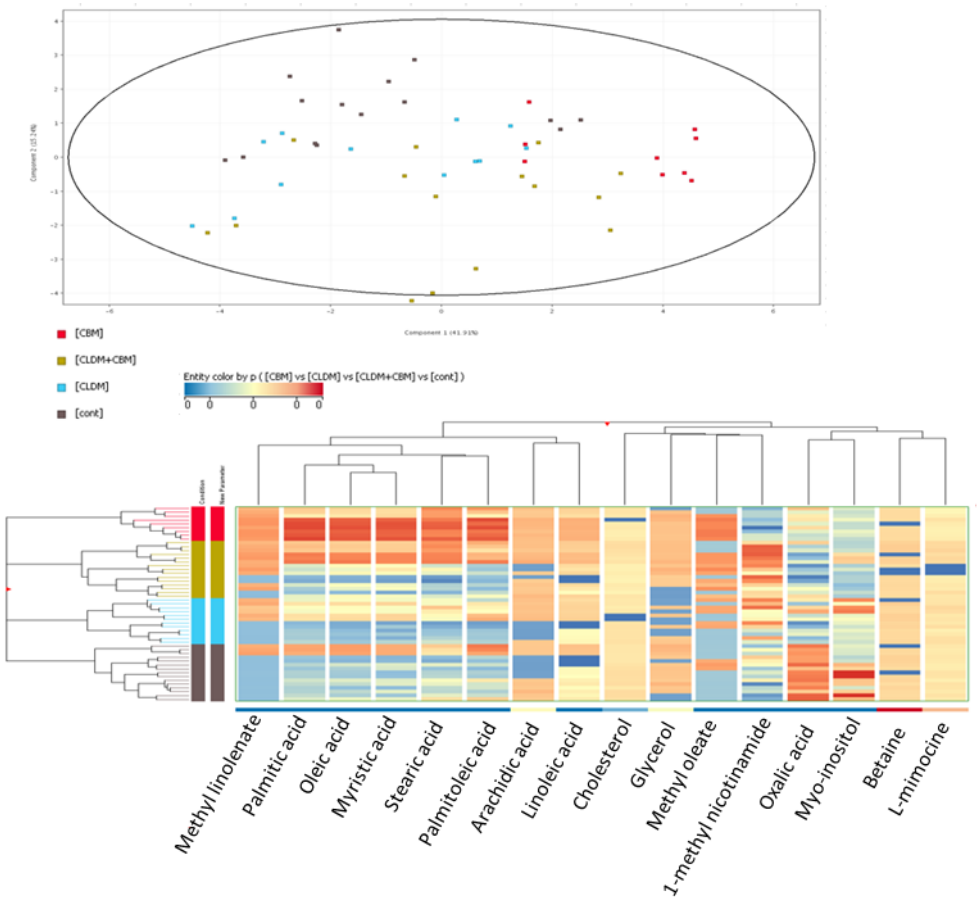

Table S1. Primers used for quantitative real-time RT-PCR, Related to Figure 3

Name	Sequence	Reference
ß-Actin	Forward (5'→3'): GTGCCGCCTGGAGAAACC	Zheng et al., 2017
	Reverse (5'→3'): GGTGGAAGAGTGGGAGTTGC	
TGF-ß$_1$	Forward (5'→3'): GTGCCTATGTCTCAGCCTCTT	Behrouzifar et al., 2018
	Reverse (5'→3'): ATTTGGGAACTTCTCATCCCT	
TLR-2	Forward (5'→3'): CAGACAAAGCGTCAAATCTCAG	Dehghan et al., 2018
	Reverse (5'→3'): AGAAGCATCACATGACAGAGACT	
TNF-α	Forward (5'→3'): TGGTGACCAGGCTGTCGCTACA	Zheng et al., 2017
	Reverse (5'→3'): TACAGTCACGGCTCCCGTGGG	
IL-1ß	Forward (5'→3'): TAGACAACTGCACTACAGGCTCCGA	Pang et al., 2017
	Reverse (5'→3'): GGGTCCGACAGCACGAGGCT	
IL-6	Forward (5'→3'): ACAAAGCCAGAGTCCTTCAGA	Zheng et al., 2017
	Reverse (5'→3'): GGTCCTTAGCCACTCCTTCTG	
COX-2	Forward (5'→3'): GGTGGAGAGGTGTATCCCCC	Lee et al., 2009
	Reverse (5'→3'): ACTTCCTGCCCCACAGCA	
INF-γ	Forward (5'→3'): CACTGCATCTTGGCTTTGCA	Liu et al., 2018
	Reverse (5'→3'): GCTGATGGCCTGATTGTCTTTC	
IL-10	Forward (5'→3'): CAACCCAAGTAACCCTTAAAGT	Dehghan et al., 2018
	Reverse (5'→3'): AGCTGCGGACTGCCTTC	
NF-κB	Forward (5'→3'): GTGGAGGCATGTTCGGTAGTG	Zheng et al., 2017
	Reverse (5'→3'): TCTTGGCACAATCTTTAGGGC	
HSP-70	Forward (5'→3'): CAAGAGGAAGCACAAGAAGGA	Behrouzifar et al., 2018
	Reverse (5'→3'): GATGTGTAGAAGTCGATGCCC	
IL-17A	Forward (5'→3'): ACTCTCCACCGCAATGAAG	Dehghan et al., 2018
	Reverse (5'→3'): TTCAGGACCAGGATCTCTTG	
MUC-2	Forward (5'→3'): TTT CAA GCA CCC CTG TAA CC	Song et al., 2018
	Reverse (5'→3'): AGG TCC TGG TGT TGA ACC TG	
ZO-1	Forward (5'→3'): ACT ATG ACC ATC GCC TAC GG	Song et al., 2018
	Reverse (5'→3'): GGG GAT GCT GAT TCT CAA AA	
OCLN	Forward (5'→3'): CGG TAC AGC AGC AAT GGT AA	Song et al., 2018
	Reverse (5'→3'): CTC CCC ACC TGT CGT GTA GT	
CLDN4	Forward (5'→3'): GGG GAT CAT CCT GAG TTG TG	Song et al., 2018
	Reverse (5'→3'): CAC TGC ATC TGA CCT GTG CT	

TGF-ß$_1$: Transforming growth factor-ß, TLR-2: Toll like receptor-2, TNF-α: Tumor

necrosis factor-α, IL-1β: Interleukin-1β, IL-6: Interleukin-6, COX-2: Cyclooxygenase-2, INF-γ: Interferon-γ, IL-10: Interleukin-10, NF-κB: Nuclear factor-kappa B, HSP-70: Heat shock protein-70, IL-17A: Interleukin-17A, MUC-2: Secretory protein mucin-2, ZO-1: Zonula occludens-1, OCLD: occludin, CLDN4: claudins-4.

Supplemental References

Behrouzifar, S., Vakili, A., and Barati, M. (2018). The Effects of Mouse Recombinant Resistin on mRNA Expression of Proinflammatory and Anti-Inflammatory Cytokines and Heat Shock Protein-70 in Experimental Stroke Model. J. Stroke Cerebrovasc. Dis. 27, 3272-3279.

Caporaso, J.G., Bittinger, K., Bushman, F.D., DeSantis, T.Z., Andersen, G.L., and Knight, R. (2010). PyNAST: a flexible tool for aligning sequences to a template alignment. Bioinformatics 26, 266-267.

Dehghan, P., Tolouie, S., Baradaran, B., Nami, S., and Morovati, H. (2018). TLR-2, IL-10 and IL-17-mediated immunity in experimental chemotherapy murine model of systemic candidiasis; cyclophosphamides' impact and roles. Microb. Pathog. 119, 183-192.

DeSantis, T.Z., Hugenholtz, P., Larsen, N., Rojas, M., Brodie, E.L., Keller, K., Huber, T., Dalevi, D., Hu, P., and Andersen, G.L. (2006). Green genes, a chimera-checked 16S rRNA gene database and workbench compatible with ARB, Appl. Environ. Microbiol. 72, 5069-5072.

Edgar, R.C. (2010). Search and clustering orders of magnitude faster than BLAST. Bioinformatics 26, 2460-2461.

Gupta, J., del Barco Barrantes, I., Igea, A., Sakellariou, S., Pateras, I.S., Gorgoulis, V.G., Nebreda, A.R. (2014). Dual function of p38α MAPK in colon cancer: suppression of colitis-associated tumor initiation but requirement for cancer cell survival. Cancer Cell 25,484-500.

Hagihara, M., Yamashita, R., Matsumoto, A., Mori, T., Kuroki, Y., Kudo, H., Oka, K., Takahashi, M., Nonogaki, T., Yamagishi, Y., et al. (2018). The impact of Clostridium butyricum MIYAIRI 588 on the murine gut microbiome and colonic tissue. Anaerobe 54, 8-18.

Langille, M.G., Zaneveld, J., Caporaso, J.G., McDonald, D., Knights, D., Reyes, J.A., Clemente, J.C., Burkepile, D.E., Vega Thurber, R.L., Knight, R. et al. (2013). Predictive functional profiling of microbial communities using 16S rRNA marker gene sequences. Nat. Biotechnol. 31, 814-821.

Lee, H., Ahn, Y.T., Lee, J.H., Huh, C.S., and Kim, D.H. (2009). Evaluation of anti-colitic effect of lactic acid bacteria in mice by cDNA microarray analysis. Inflammation 32, 379-386.

Liu, Z., Lai, K., Xie, Y., He, X., and Zhou, X. (2018). Gli2 Mediated Activation of Hedgehog Signaling Attenuates Acute Pancreatitis via Balancing Inflammatory Cytokines in Mice. Cell Physiol. Biochem. 48, 120-130.

Pang, M., Yuan, Y., Wang, D., Li, T., Wang, D., Shi, X., Guo, M., Wang, C., Zhang, X., Zheng, G., et al. (2017). Recombinant CC16 protein inhibits the production of pro-inflammatory cytokines via NF-κB and p38 MAPK pathways in LPS-activated RAW264.7 macrophages. Acta. Biochim. Biophys. Sin. 49, 435-443.

Song, C.H., Kim, N., Sohn, S.H., Lee, S.M., Nam, R.H., Na, H.Y., Lee, D.H., Surh, Y.J. (2018). Effects of 17β-Estradiol on Colonic Permeability and Inflammation in an Azoxymethane/Dextran Sulfate Sodium-Induced Colitis Mouse Model. Gut Liver 12, 682-693.

Tachi, M., Kondo, F., Fukayama, M., Yoshikawa, K., Matsuura, K., and Okada, S. (2014). Mass spectrometric determination of prostanoids in rat hypothalamic paraventricular nucleus microdialysates. Auton Neurosci. 181, 49-54.

Yamazaki, K. (1988). Study on selective medium for isolation of Clostridium butyricum from human feces, MEDICIN and BIOLOGY 116, 227-230.

Zheng, L., Zhang, Y.L., Dai, Y.C., Chen, X., Chen, D.L., Dai, Y.T., and Tang ZP. (2017). Jianpi Qingchang decoction alleviates ulcerative colitis by inhibiting nuclear factor-κB activation. World J. Gastroenterol. 23, 1180-1188.